Journal of Simulation and Analysis of Novel Technologies in Mechanical Engineering
16 (2) (2024) 0005~0032
DOI 10.71939/jsme.2024.1120195

Review paper

An overview of friction stir processing of magnesium alloys reinforced by ceramic additive: microstructure and mechanical Properties

Masoud Kasiri-Asgarani*
Advanced Materials Research Center, Department of Materials Engineering, Najafabad Branch, Islamic Azad University, Najafabad, Iran.
*m.kasiri.a@gmail.com, m.kasiri@pmt.iaun.ac.ir

(Manuscript Received --- 18 May 2024; Revised --- 08 July 2024; Accepted --- 21 July 2024)

Abstract

The aerospace, automobile, electronics, and biomedical sectors are just a few of the industries that have made substantial use of magnesium (Mg) alloys because of their outstanding specific strength and stiffness, strong vibration absorptionf, electromagnetic shielding impact, superior machinability, and recyclability. Surface metal matrix composites (SMMCs) are a class of contemporary manufactured substances in which the material's core retains its chemical composition and structure while its surface is altered by the dispersion of secondary phase in the shape of fibers or particles. Friction Stir Processing (FSP) is a cutting-edge method for creating composites that achieves significant grain refinement. Numerous studies have noted improvements in the tribological, microstructure, and mechanical characteristics of magnesium metal matrix composites (MMMCs) made via the FSP process. Currently, the most common types of magnesium alloys consist of RZ5, AZ31, AZ61, AZ91, ZM21, ZK60, and pure magnesium. Carbon nanotubes (CNTs), graphene, carbon fiber, SiC, SiO_2, Al_2O_3, B_4C, TiC, and ZrO_2 particles are some examples of the reinforcing particles. The primary mechanisms for the joining and grain refinement throughout FSP of Mg alloys are outlined. It is discovered that the FSP treatments change the attributes including tensile strength, hardness, wear and corrosion resistance, and that the type of ceramic particle reinforcement greatly affects the extent of the changes. The principles, technology, microstructure, mechanical characteristics, tribological, and corrosion performance of magnesium and its alloys employing ceramic particle reinforcements are summarized in this paper.

Keywords: Friction Stir Processing, Magnesium, Microstructure, Mechanical Properties, Ceramic Particles.

1- Introduction

It is common knowledge that adding alloying elements, metal fibers, or powders of different sizes and compositions to metal parts may boost their strength. Since the 1980s, this topic became the subject of much research. In the last ten years, a lot of focus is being placed on techniques including FSP, cold spraying, laser melting, ion implantation, and plasma spraying that create subsurface gradient structures in metallic materials [1-3]. "The Welding Institute (TWI)" created friction stir welding (FSW) in 1991. It is employed in the procedure of joining alloys or metals that are identical and distinct. A cylindrical tool with a shoulder and pin in FSW helps to provide adequate heat to facilitate the joining of materials. It was really challenging to fuse the different materials together prior to FSW. The manufacturing sectors were able to attach copper to aluminum, separate aluminum series, etc. more easily thanks to the assistance of FSW. As FSW advanced, a number of opportunities emerged. Among the variations of friction stir welding are friction stir processing (FSP) and FSW [4-6]. FSP was created in 1999 by Mishra et al. utilizing the fundamental idea of FSW. A rotating and traversing tool is part of the basic FSP configuration. The tool receives both a downward push and a spinning movement. Once the tool shoulder makes contact with the sample surface, the revolving

tool pin sinks farther into the material being worked on. The sample undergoes significant plastic deformation due to heat generated by friction among the tool and the sample. The workpiece material passes from the advancing part over to the receding part of the sample in conjunction with the tool's stirring operation. It was discovered that FSP is appropriate for a number of applications, including surface composite production, microstructure modification in cast alloys, and casting defect removal. The base metal's super-plasticity and grain refining are aided by the stirring operation. The localized flaws in the cast and forged materials are eliminated using FSP. It alters the microstructure and eliminates the imperfections brought on by pores and fissures. The material's superplasticity is aided by the creation of equiaxed recrystallized grains. The recrystallized grains that result from the tool's swirling movement are aided by FSP. Numerous investigators examined FSP and discovered that the surface composite possesses enhanced tribological, microstructural, and mechanical characteristics [7-11].

The material undergoes localized softening throughout FSP as a result of adiabatic heating caused by plastic deformation throughout material flow, as well as heat produced by friction between the tool and the sample. The shoulder controlled the heat production because its region of contact and vertical pressure were far greater compared to those between the pin and the sample, and its linear velocity was greater compared to the pin's smaller radius [12]. Material is being stirred and mixed within the revolving pin by the tool's rotation, and the stirred material is moved from the pin's front to its back by the tool's translation. The instrument may be angled somewhat in the path of the trailing motion (the spindle angle) for this reason [13]. Because of this, at high temperatures, the material in the stirred zone (SZ), commonly referred to as the nugget or dynamically recrystallized (DRX) zone, experiences significant plastic deformation, which leads to the creation of a fine DRX microstructure [14-17]. More information on the many DRX mechanisms that have been described in this regard, including continuous (CDRX), discontinuous (DDRX), geometric (GDRX), and twinning (TDRX), can be obtained in current review studies [14, 18]. A thermo-mechanically affected zone (TMAZ, a deformed area affected via heating and deformation) [19] and a heat-affected zone (HAZ, resulting from going through a thermal cycle) will emerge as well from SZ to the base metal (BM), as illustrated in Fig. 1i(a) [20]. Similar to SZ, the TMAZ deforms, but because there is not enough strain at this zone, recrystallization does not happen entirely [18]. With the feasible exception of minor grain coarsening and the potential dissolving of strengthening precipitates, the microstructure of HAZ is nearly comparable to that of base metal. [13, 21, 22].

2- Friction Stir Processing

As seen graphically in Fig. 1i, FSP is performed by pressing a rotating friction stir tool—which consists of a cylindrical shoulder and a protruding, tightly positioned pin or probe—into the workpiece's surface, accompanied by its translational motion. During the plunge phase, the rotating tool is first pushed into the material by the pin penetrating the workpiece and the shoulder making contact with the surface. Once the requisite plunge depth was reached, the instrument is left in place long enough to attain the necessary temperature, after which the dwell, or stabilization phase, starts.

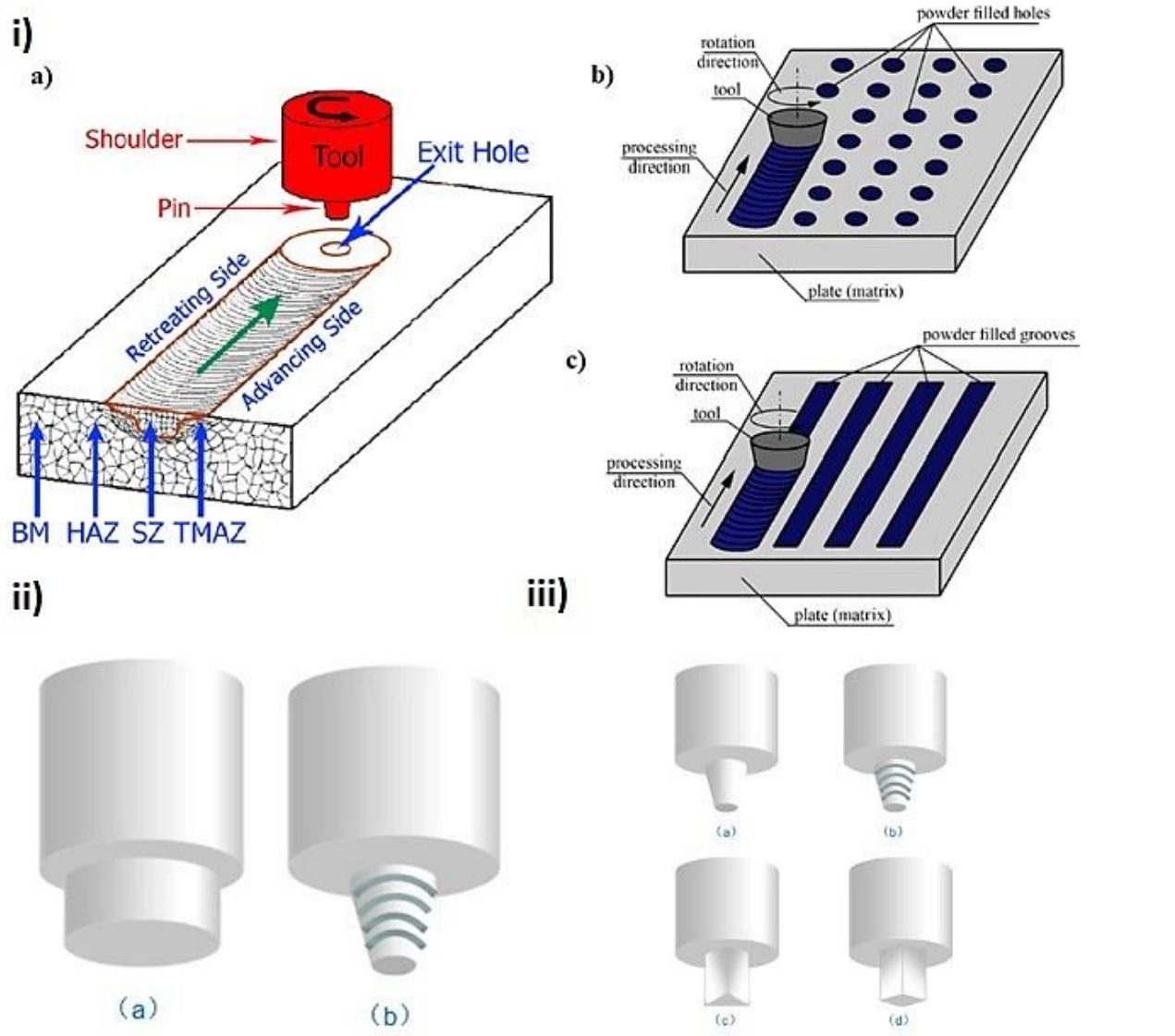

Fig. 1 Schematics of: **a)** FSP and the resulting microstructural regions [20], the reinforcements filled into b) holes and c) grooves [23], ii) Two common kinds of stir tools: (a) pin-less and (b) with pin, and iii) Different shapes of pin: (a) circular; (b) circular with thread; (c) triangular; and (d) square [11]

The material is subsequently processed by the tool's translational motion throughout the advancing phase. Additionally, the shoulder forges downward, preventing the deformed material from being expelled from the treated area. In the retraction phase, the instrument is ultimately withdrawn at the last stage of processing [2-5, 11].

There are two types of non-consumable stir tools employed in the FSP procedures: pin-less and pin-equipped (Fig. 1 ii). Pin-less tools are typically employed for embedding reinforced particles throughout composite manufacturing, while pin-equipped tools tend to be employed for changing material surfaces. The heat generation and material flow throughout FSP operation are significantly influenced by the dimensions of the tool and the pin's shape. The material plastic deformation is more severe and the friction heat is focused once a tool with a bigger shoulder diameter is employed. As consequence, the second phase particle refinement and microstructure stability are improved. Research regarding the way pin profiles affect heat production throughout the

plunge step reveals that a successful instrument pin area is crucial for both heat generation and friction deformation; as a result, using a conical pin throughout the plunge step results in the lowest temperature. The common kinds of tools employed in FSP for magnesium-based alloys are displayed in Fig. 1 iii. [20, 23].

The various FSP process variables are displayed in Fig. 2 [24]. Three categories — machine factors, tool variables, and reinforcing material—are used to group the FSP variables. FSP is a multifaceted technique that combines metallurgical contact, plastic deformation, and heating. Therefore, in order to attain the intended surface increase, it is essential to determine the impact of every variable.

The FSP of particle-reinforced materials has gained popularity over the past ten years. Using metallic alloys as a base, this manufacturing technique creates surface composite coatings with a typical thickness ranging from 50 to 600 μm. For the surface composites, the reinforcing additions can be fibers, platelets, or powder. When necessary, blind holes are typically drilled on the highest point of the sample in a straight or zigzag pattern and filled with reinforce particles. This technique is known as "hole filling." To prevent these particles from scattering, a pin-less FSP tool is used following the loading of reinforced particles prior to the ultimate testing fragments. Another popular approach is groove filling, which involves creating a region on the sample and loading it with reinforced particles. To prevent these particles from dispersing, a pin-less FSP instrument is used following the loading of reinforced particles prior to the ultimate testing [23]. The aerospace, automotive, electronics, and biomedical areas are just a few of the sectors that have made substantial use of magnesium (Mg) alloys because of their outstanding specific strength and stiffness, strong vibration absorption, electromagnetic shielding effect

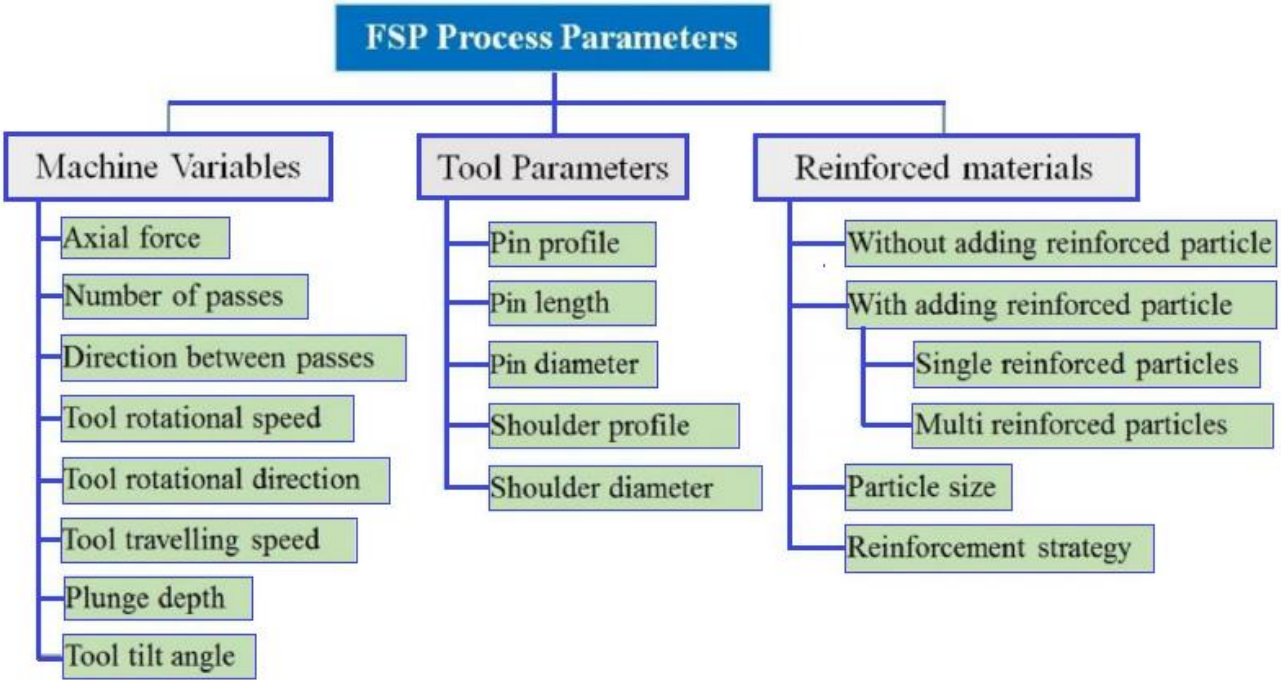

Fig. 2 Classification of FSP parameters [24].

,great machinability, and recyclability. The lightweight magnesium metal matrix composites (MMCs) are strengthened with fibers or particles. Magnesium alloys with various additional components provide for intriguing study subjects for experts [25-27]. Furthermore, because of their superior corrosion resistance and outstanding mechanical qualities, surface metal matrix composites, or SMMCs, represent a group of structural materials with great promise. In SMMCs, fibers, whiskers, and ceramic particles make up the reinforcing phase, whereas a metal matrix material makes up the matrix. Consequently, SMMCs' surface qualities—such as their hardness, strength, and resistance to wear—are greatly enhanced [28]. This paper provides an overview of the principles, technology, microstructure, mechanical characteristics, tribological characteristics, and corrosion characteristics of magnesium and related alloys when ceramic particle additives are used. Currently, pure magnesium, AZ31, AZ61, AZ91, ZM21, ZK60, and RZ5 are the primary types of magnesium alloys. The particles that serve as reinforcements comprise graphene, carbon nanotubes (CNTs), graphene fiber, SiC, SiO_2, Al_2O_3, B_4C, TiC, and ZrO_2 powder. Table 1 provides a concise overview of the work undertaken to create Mg composites supplemented with ceramic additives using the FSP method.

3- FSP with oxide ceramics reinforcement

Because of its great thermal stability and wear resistance, aluminum oxide (Al_2O_3) is a widely recognized extremely durable ceramic that is utilized in high-temperature uses including refractory, cutting instruments, and aircraft. A particularly stable phase that is frequently utilized in structural uses is the hexagonal alpha phase. Because of its superior strength, refractoriness, and hardness, it is the preferred material for a variety of purposes. A number of the key reinforcing elements in Metal Matrix Composites (MMCs) is ZrO_2, which has minimal density and outstanding mechanical and surface qualities that are particularly well suited for anticorrosion and wear resistance. Furthermore because of its inexpensive cost and efficient improvement of the metal matrix's tribological performance features, silicon dioxide (SiO_2) is one among the most widely used friction materials. Numerous studies looked into how to enhance the functionality and surface characteristics of Mg alloy surfaces by adding micro- and nano-particles (NPs) of these ceramics. The materials and experimental protocols for FSP using ZrO_2, SiO_2, and Al_2O_3 additive particles are displayed in Table 1.

The strategy that follows can be used to admix hard, fine-grained particles to the substrate throughout FSP. The metal matrix beneath and surrounding the tool becomes plasticized due to the heat produced by the friction between the pin and the tool shoulder. The plasticized metal matrix material is entrained by its translational and rotational movement from the approaching side to the retreating side. The compacted particles are mixed in with the plasticized metal matrix material by the flow of the matrix material, which also fractures the grooves (or holes). The degree of stirring and composite creation are determined by the tool's rotation rate and traverse speed. The plasticized metal matrix can be used with any kind of reinforcing particle to create a composite, according to an analysis of evidence from experiments. Dinaharan et al.'s [71] manufactured copper matrix composite films augmented with different ceramic particles amply illustrate this point. Their outcome demonstrated that the arrangement of particle distribution in the composite films is insensitive to the kind of ceramic

Table 1: Brief summary of the work carried out to produce Mg based surface MMCs by FSP as reported in the literature

Reinforced Phase	Base Materials	Shape/Average Particle Size	Method	Rotational Speed (ω) (rpm)	Traverse Speed (V) (mm/min)	Pin or probe Shape	Tool Material	Tool Dimensions Shoulder Diameter/Pin Diameter/ Length of Pin (mm)	Tool Tilt Angle (°)	Maximum FSP number of passes	Main Results	Average grain size of the Base Alloy (before FSP)/minimum of Grain Size after FSP (μm)	Ref.
ZrO_2	AZ31	Particles/ 50-150 nm in diameter	Hole	1180	23.5	Cylindrical	-	20/4/2	2	4	The corrosion resistance, UTS and YS: FSP-4Pass>Basese Metal> FSP-2Passese	10/4.5	[29]
	AZ91D	Particles/ 50 μm in diameter	Groove	900	20	Cylindrical	HCHCr steel	16/6/4	-	1	The corrosion rate of the developed surface composite was ~78% less than that of the base material.	-/-	[30]
	AZ31	Particles/ 40 nm in diameter	Groove	1250	20	Cylindrical	H13	14/6/2	-	4	distributed uniformly in the magnesium matrix without the formation of clusters/	40/4	[31]
	AZ31	Particles/ 50 nm in diameter	Groove	9000	200	Cylindrical	-	7/-/1.9	3	3	The agglomeration of ZrO2 particles reduced with the increase of FSP passes	-/8.23	[32]
	AZ31	Particles/ 80 nm in diameter	Hole	1180	23.5	Cylindrical	-	20/2/4	2	6	Grain refinement / increased the hardness, UTS, YS/ the icorr of FSP-ZrO2 composites decreases and the radius of capacitive loop increases,	10/3.2	[33]
	AZ31B	Particles/ 8 nm in diameter	Groove	800-1200	100	Cylindrical	H13	18/6/4.7	3	1	Grain refinement / increased the hardness, UTS, YS/ the icorr of FSP-ZrO2 composites decreases	-/2.49	[34]
	AZ31	Particles/ 20-50 nm in diameter	Groove	1500	50	Cylindrical	-	16/4/3.8	2.5	1	fine uniform equiaxed crystal grains/ better damping capacities	-/10.29	[35]
	AZ31	Particles/ 30-40 nm in diameter	Hole	1000	56	Threaded cylindrical pin	AISI 52100 steel	16/4.3/4	2	4	Grain refinement/ / increased the hardness/ reduced the friction coefficient	10.7/2.1	[36]
	AZ31B	Particles/ 8 μm in diameter	Groove	800	100	Cylindrical	H13	-/-/-	-	4	The microstructure, tensile, hardness,wear, and corrosion responses of the composites were investigated	-/3.02	[37]

Reinforced Phase	Base Materials	Shape/Average Particle Size	Method	Rotational Speed (ω) (rpm)	Traverse Speed (V) (mm/min)	Pin or probe Shape	Tool Material	Tool Dimensions Shoulder Diameter/Pin Diameter/ Length of Pin (mm)	Tool Tilt Angle (°)	Maximum FSP number of passes	Main Results	Average grain size of the Base Alloy (before FSP)/minimum of Grain Size after FSP (μm)	Ref.
`Al_2O_3	AZ31	Nano Particle/ 50 nm	Groove	1050	33.4	Cone	-	20/(3.5d-5.5D)/5h	0.5	4	More corrosion resistant in wear	-	[38]
	AZ91	Nano Particle/ 50 nm	Groove	500-2000	20-80	Cylindrical	H21	20/4.5/4.5	3	1	increased the hardness 30%/ reduced of friction coefficient/ reduced the mass loss	45/ 3.6	[39]
	AZ91	Nano Particle/ 30 nm	Groove	900	63	Square		15/3.5×3.5)/2.5	3	6	more resistant in wear/ matrix finer grains/ higher hardness, strength, elongation	150/7	[40]
	AZ31	Nano Particle/ 30 nm	Groove	800-1400	45	Cylindrical	H13	18/6/5.6	2	4	wear resistance/ changed the wear mechanism	70/3	[41]
	AZ31	Nano Particle/ 35 nm	Groove	800-1200	45	Cylindrical	H13	18/6/5.7	2	4	higher hardness/ particles distribution	70/2.2	[42]
	AZ91	Nano Particle/ 3000, 300 and 30 nm	Groove	900	63	Triangular Square	H13	15/5/1.8	3	3	The grain size and cluster size in the specimen produced by the triangular tool is smaller than that of square tool.	150/1.7 for Triangular Tool 150/2.5 for Square Tool	[43]
	Pure Mg	Nano Particle/ 50 nm	Groove	800	50	Cylindrical	H13	13.6/5/3.7	2.5	4	improved hardness and wear resistance/ Wear resistance of two passes was higher than the four passes	-/1.3	[44]
SiO_2	AZ31B	Particles/ 20-30 nm in diameter	Groove	1250	50	Taper	H13	17/(4.5d-5.5D)/2.5	-	4	Chemical reaction occurred at Mg/SiO2 interface to form Mg2Si and Si/ composite samples had a randomly oriented texture	335/6.7	[45]
	AZ61A	Particles/ 20 nm in diameter	Groove	800	45	-	-	-/-/-	2	4	high strain superplasticity over 400%	75/0.5-2	[46]
	AZ31	Particles/ 20 nm in diameter	Groove	800	45	Cylindrical	-	18/6/6	2	4	Improve The hardness and tensile properties at room temperature	70/2-4	[47, 48]
	AZ91	Particles/ 20 nm in diameter	Groove	1250	20-63	Square	H13	15/(4.54×4.54)/4	3	3	Increased traverse speed has effect on the mechanical behavior of the composite/	140/8.27	[49]

Reinforced Phase	Base Materials	Shape/Average Particle Size	Method	Rotational Speed (ω) (rpm)	Traverse Speed (V) (mm/min)	Pin or probe Shape	Tool Material	Tool Dimensions Shoulder Diameter/Pin Diameter/ Length of Pin (mm)	Tool Tilt Angle (°)	Maximum FSP number of passes	Main Results	Average grain size of the Base Alloy (before FSP)/minimum of Grain Size after FSP (μm)	Ref.
SiC	AZ91	Particles/ 30 μm in diameter	Hole	400-750	50	Taper	H13	20/(4d-6D)/4	2	1	Grain refinement	110/11	[50]
	Pure Mg	Particles/ 100-150 μm in diameter	Hole	600-800	30-50	Cylindrical	H13	18/6/5.7	0	1	Taguchi model was used to optimize FSP parameters	-/-	[51]
	Pure Mg	Particles/ 35μm in diameter	Melting	1000-1600	50	Cylindrical	H13	16/5/4.7	-	1	Reduction the grain size/ porosity elimination/ breakage of reinforcement clusters/uniform distribution of SiC particles/increased microhardness	705/3	[52]
	AZ31	Particles/ 60 nm and 1 μm in diameter	Groove	950	47.5	Cylindrical	H13	16/4/5	-	4	Grain refinement /increased the tensile strength	-/2.5	[53]
	AZ31B	Particles/ 250 μm in diameter	Groove	800-2000	25-200	Cylindrical	H13	16/5/4	-	1	very sensitive to the process parameters (the rotational and translational speeds and the groove geometry)/ significant increase in the microhardness	13.1/1.46	[54]
	Pure Mg	Particles/ 35 μm in diameter	Melting	1300	50	Cylindrical	-	16/5/4.7	0	1	reduction the grain size/ reduced SiC particles size	170/3	[55]
	RZ5	Particles/ Nano	Hole	500-700	30-60	Cylindrical	-	19/6/4/-	1	2	enhanced the tensile strength/ tool traverse rate has significant effect on tensile strength and abrasive wear characteristics	-/-	[56]
	AZ31	Particles/ 30 μm in diameter	Groove	1500	25-200	Cylindrical	SKD61	12/4/8	3	4	Increased the microhardness/ refined the grain/ maintained grain size maintained at the elevated temperatures (~400 ◦C)/	79.1/6	[57]
	AZ91	Particles/ 50 nm in diameter	Groove	700-1250	12.5-45.5	Cylindrical	WC	20/6/-	-	1	vibration and process parameters has significat on microstructure and mechanical characteristics	150/7.17	[58]

Reinforced Phase	Base Materials	Shape/Average Particle Size	Method	Rotational Speed (ω) (rpm)	Traverse Speed (V) (mm/min)	Pin or probe Shape	Tool Material	Tool Dimensions Shoulder Diameter/Pin Diameter/ Length of Pin (mm)	Tool Tilt Angle (°)	Maximum FSP number of passes	Main Results	Average grain size of the Base Alloy (before FSP)/minimum of Grain Size after FSP (µm)	Ref.
	AZ91	Particles/ 30 nm and 5µm in diameter	Groove	710	40	Square		15/(3.5×3.5)/2.5	3	2	The effect of nano-sized SiC particles on the grain size and hardness of the fabricated layer is found to be more impressive than micro-sized particles/ Increasing the rotational speed increases the grain size as the hardness decreases	150/5	[59]
	AZ91	Particles/ 30 and 300 nm in diameter	Groove	700-1250	12.5-45.5	Cylindrical	WC	20/6/-	2	1	Hardness, strength, and ductility of FSV processed Specimens, were higher than those of FS-processed specimen.	-/-	[60]
TiC	Pure Mg	Particles/ 45 µm in diameter	Hole	600	15	Cylindrical	Stainless Steel	16/3/1.6	-	3	increased the hardness, microhardness, wear resitante	84/7	[61]
	AZ31	Particles/ 5 µm in diameter	Groove	1250	50	Cylindrical	H13	14/6/-	2.5	1	increased the hardness	40/12	[62]
	AZ31B	Particles/ 4 µm in diameter	Groove	1200	40	Cylindrical	HCHCr steel	18/6/5	-	1	distributed uniformly in the magnesium matrix without the formation of clusters/There was no interfacial reaction between the magnesium matrix and the TiC particle/TiC particles were properly bonded to the magnesium matrix.		[63]
	AZ61A	Particles/ 80 nm in diameter	Hole	800-1200	40	Cylindrical	HCHCr steel	16/6/4	-	3	Grain refinement / increased the hardness, microhardness, wear resitante	75/4	[64]
	AZ61A	Particles/ 80 nm in diameter	Hole	850	25-170	Triangle	HCHCr steel	21/-/4	-	3	There were no chemical reaction seen between TiC particles and parent metal	-/-	[65]

Reinforced Phase	Base Materials	Shape/Average Particle Size	Method	Rotational Speed (ω) (rpm)	Traverse Speed (V) (mm/min)	Pin or probe Shape	Tool Material	Tool Dimensions Shoulder Diameter/Pin Diameter/ Length of Pin (mm)	Tool Tilt Angle (°)	Maximum FSP number of passes	Main Results	Average grain size of the Base Alloy (before FSP)/minimum of Grain Size after FSP (μm)	Ref.
B_4C	AZ91	Micro Particle/ 10-15 μm	Groove	1400	25	Square	-	15/(4.25D-2d)/3	0	1	improved hardness and wear resistance/ Wear resistance	166.5/12.5	[66]
	AZ91	Micro Particle/ 50, 20 and Submicron μm	Drilled Holes	900	45	Cylindrical	Mild Steel	12/4/4	0	1	improved hardness and wear resistance/ Microhardness was increased with the increase in particle size	-/-	[67]
Carbon Nano Tube (CNT)	AZ31B	CNT/ 10-30 nm in diameter and 1-25 μm in length	Groove	715-1400	25-210	Cylindrical screw-shap	SKD61 steel	16/4/4	3	2	increased the hardness 70%/	19/3	[68]
	AZ91	CNT in Cu Matrix	Groove	1500	15-50	Cylindrical	Tungsten Carbide	12/4/1.3	0	1	good interfacial bonding/ enhanced the tensile strength/ improved the microhardness	-/-	[69]
	Mg-6Zn	CNT/ 40-60 nm in diameter and 2 μm in length	Melting	1000	50	Cylindrical	-	15/3/4.5	1.5	1	Grain refinement/	-/4.4	[70]
	AZ91D	CNT/ 10-20 nm in diameter and 30 μm in length	Hole	950	30	Cylindrical	-	26.8/12/7.8	0	1	no significant influence on grain refinement/ increased the yield strength and elastic modulus,	-/-	[71]
	AZ31	CNT/ 20-50 nm in diameter and 10-20 μm in length	Groove	1000	28	Cylindrical		18/7/4	-	4	increased the yield stress/ decreased the ultimate stress and elongation.	-/1.15	[72]
	AZ31B	MWCNT/10-30 nm in diameter and 10- μm in length		1000-1400	40	Cylindrical	H13	18/5/5.5	2	3	Increased the tensile strength and compressive strength with the increase in rotation speed/	-/-	[73]
	AZ31	MWCNT/10-30 nm in diameter and 10- μm in length	Hole	1600	40	Cylindrical	H13	18/5/5.5	2	4	no interfacial reaction between the Graphene with AZ31Mg/ Increased the tensile strength and compressive strength	53/4.2	[74]

Reinforced Phase	Base Materials	Shape/Average Particle Size	Method	Rotational Speed (ω) (rpm)	Traverse Speed (V) (mm/min)	Pin or probe Shape	Tool Material	Tool Dimensions Shoulder Diameter/Pin Diameter/ Length of Pin (mm)	Tool Tilt Angle (°)	Maximum FSP number of passes	Main Results	Average grain size of the Base Alloy (before FSP)/minimum of Grain Size after FSP (μm)	Ref.
Graphen	AZ31	Single layer plate/ 1 nm thickness and 2-10 nm in diameter	Hole	1000	60	-	-	18/5/3.85	-	1	increased the UTS and elongation (15.7%)	76.81/7.73	[75]
	AZ31B	Single layer plate/ 3-6 nm thickness and 5-10 nm in diameter		1000-1400	40	Cylindrical	H13	18/5/5.5	2	3	Increased the tensile strength and compressive strength with the increase in rotation speed/	-/-	[73]
	AZ31	Single layer plate/ 3-6 nm thickness and 5-10 nm in diameter	Hole	1600	40	Cylindrical	H13	18/5/5.5	2	4	no interfacial reaction between the Graphene with AZ31Mg/ Increased the tensile strength and compressive strength	53/4.2	[74]
Carbon Fiber	AZ91	Fiber/ 8 μm Diameters	Groove	1400	100	Threaded pin/ 3-Flat pin		18.5/-/4.7	3	1	3- flat pin decreased the size and number of defects and fatigue strength	450/9	[76]

particles used. A non-uniform particle distribution is not caused by either the density gradient or the copper matrix's propensity to make ceramic particles wettable. It is also observed that because of the temperature differential throughout the plate's depth, layers with a large and small content of ceramic particles occur as a result of a combination of the material flows induced separately by the tool shoulder and the pin.

In the region of the stir, where reinforcing particles are found within the grains and at the grain borders, severe plastic deformation and DRX throughout FSP produce a small equiaxed grain [61,63,71,76]. No interfacial reactions were seen when reinforcement particles were incorporated into the matrix via FSP; instead, a clear border between the matrix and the newly added particles was detected, as demonstrated, for example, in Fig. 3 for AA6063 alloy FSPed with the inclusion of vanadium particles [63]. The vanadium particles and the aluminum matrix are clearly defined by the composite image exhibited in Fig. 3. In addition to the matrix and particle reaction levels, none of the other reaction layers in Fig. 3b would exhibit contrast. The results of the EDX line scan verify this.

3-1- Microstructure evaluation of Mg-based containing ZrO_2, SiO_2, and Al_2O_3

Using reinforced particles, the structure and composition of BM could be altered throughout FSP. AZ31/ZrO_2 nanocomposites (NC) exhibiting excellent homogeneity were effectively synthesized by FSP, as reported by Qiao et al. [33]. Grain refining of the magnesium alloy is achieved through the incorporation of ZrO_2 particles and DRX. The inverted pole Fig. (IPF) of the BM, FSP, and FSP-ZrO_2 specimens are displayed in Fig. 4(i) A–C. Equiaxed grains with an average size of 10 µm are seen in BM. When in comparison with BM, FSP exhibits a finer grain along with a more homogeneous microstructure, with an average grain size of 4.0 mm and a range of 0.1–15 mm Fig. 4(i)B. With an average grain size of 3.2 mm and a spectrum of 0.1–14 µm, the microstructure of the FSP-ZrO2 specimen is further refined and uniformed, suggesting that ZrO_2 particles help reduce grain size. The distribution of Zr elements in the FSP-ZrO_2 sample is displayed in Fig. 4(i) D. Following FSP, the ZrO_2 particles have even distribution in the composites because the Zr element is evenly distributed in the Mg matrix without any visible voids or aggregation. Because

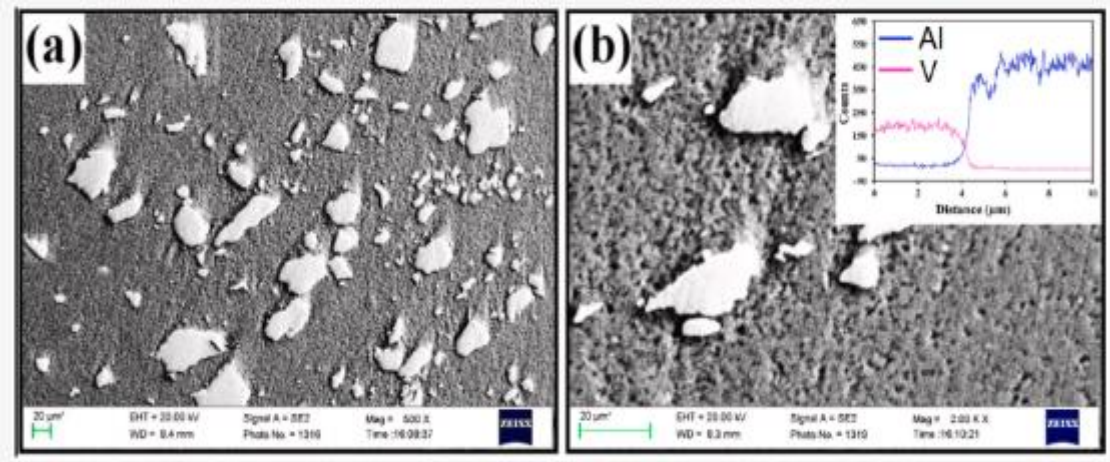

Fig. 3 Microstructure of FSPed AA6063 with 12 vol. % V content at magnification: (a) 500× and (b) 2000× (the insert shows the EDX line scan along the particle interface) (reproduced from [7]

there is an enormous variance between the elastic modulus of the ZrO_2 particles and the Mg matrix, upon FSP, the stress is localized close to the ZrO_2 particles, causing many dislocations to form surrounding them. Conversely, the relatively small stacking fault energy of magnesium alloys reduces the dynamic recovery and causes both compact and sparse dislocations.

The nano ZrO_2-encapsulated AZ31 alloy composites were made by Zang et al. [32] using high rotation speeds, three multi-passes, and varying volume fractions of the nano-ZrO_2 reinforcement in FSP. The AZ31/ZrO_2 composites showed a small microstructure and homogeneous dispersion of ZrO_2 particles. Remarkable interfacial bonding between ZrO_2 and the magnesium matrix was discovered. The TEM images of the evenly dispersed ZrO_2 particles in the FSPed AZ31/ZrO_2 composite (Z3-3P specimen) are displayed in Fig. (4(ii) a-d), and the region that was chosen diffraction pattern is displayed in Fig. 4(ii)b. This further verifies that ZrO_2 particles are present in the Z3-3P samples. The Z3-3P specimen has evenly distributed ZrO_2 particles. The high magnification TEM micrographs are displayed in Fig. 4(ii)c, where the interface was found to be continuous and flawless (micro-voids and cracks). The ZrO_2 particle's layer-to-layer separation is roughly 0.213 nm. The interfacial area between the ZrO_2 particle and the Mg matrix is depicted in Fig. 4 (ii)d. It was noticed that there was great interfacial attachment without any reaction product. The significant plastic deformation and reduced production of heat throughout FSP are responsible for the good joining of AZ31-ZrO_2.

In order to achieve synergistic effects, Liu et al. [34] inserted a combination of rare-earth CeO_2 and ZrO_2 particles into the structural AZ31B magnesium alloy using a multiple-tool pass method and FSP. The results show that after several tool passes, the tunnel-like flaws were eliminated and the CeO_2+ZrO_2 particles in the composite clustered because of the sequential mechanical stirring-assisted material flow. Other research on the usage of CeO_2+ZrO_2 as filler of Mg-based alloys have comparable properties with encapsulated Mg

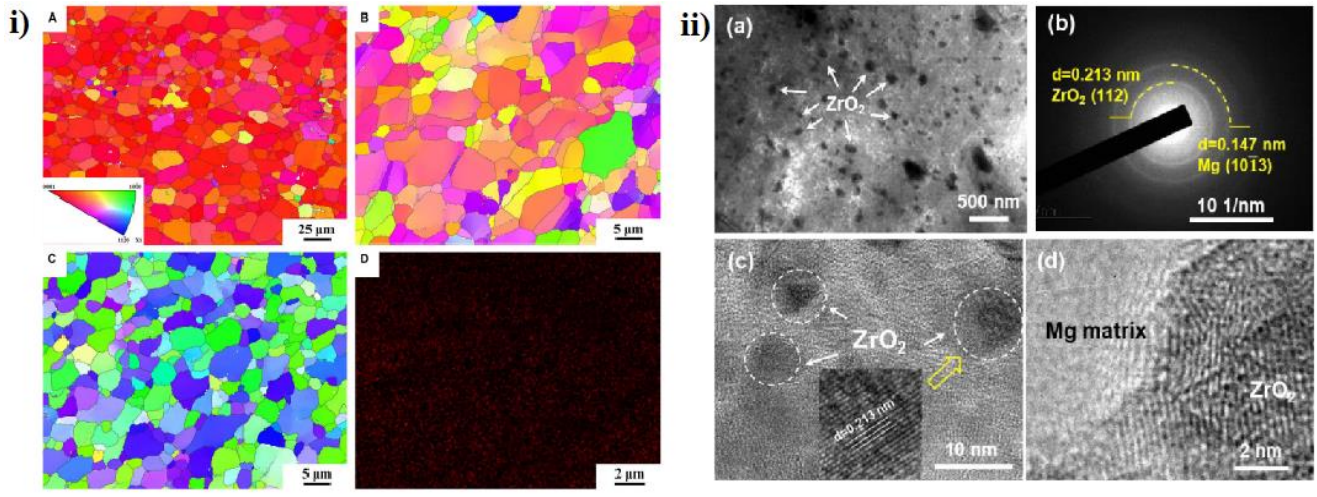

Fig. 4 i) The IPF map of (A) BM, (B) FSP and (C) FSP-ZrO_2; (D) The EDS map of FSP-ZrO_2 sample [29]; and ii) TEM images of FSPed AZ31/ZrO2 composite (Z3-3P specimen): (a) distribution of ZrO2 particles, (b) selected area diffraction pattern, (c) high-resolution TEM micrograph, and (d) interface between the Mg matrix and ZrO2 particle [32].

containing ceramic oxide [77-79]. The impact of rotational speed and probe pattern on the microstructure and strength of AZ31/Al_2O_3 NC produced by FSP is examined by Azizieh et al. [42]. Following each FSP pass, the matrix's refinement of grains and NPs dispersion were enhanced. Greater NPs dispersion is produced through elevated rotational speed since it increases the base alloy's grain size through higher heat input and rotational shattering action. Other investigations on the employing of Al_2O_3 as a great reinforcement for Mg-based alloys (Fig. 5) [44, 80-82].

By using FSP method, Lee et al. [46] created the Mg-based nano-composites AZ91/SiO_2. The outcomes indicate a substantial reduction in particle size upon boosting the traverse speed. Additionally, the MgO phase forms in part throughout the fabrication of the TEM foil and in part throughout FSP. As seen in Fig. 6, after a few passes, let's say three or four, some SiO_2 particles would combine with the magnesium matrix to generate Mg_2Si. Part of the nano-sized silica particles are hypothesized to have first changed into MgO and Si, which then reacted to produce the Mg_2Si compound. During FSP, both MgO and Mg_2Si phases, with sizes ranging from 5 to 200 nm, would develop. Similar results exhibited employing of SiO_2 particles act as a great reinforcement for Mg-based alloys [47, 48].

.

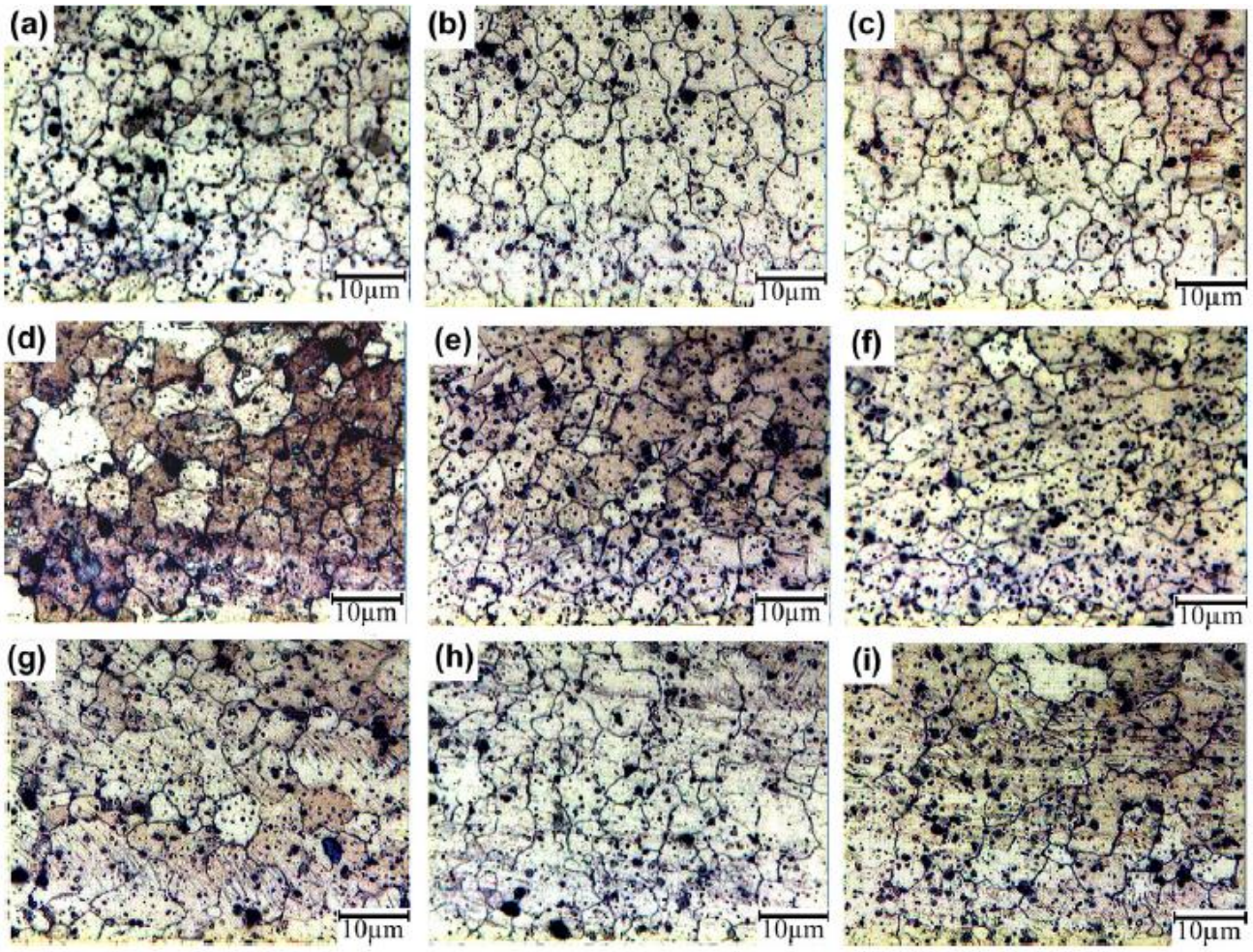

Fig. 5 Effect of rotation speed and the number of passes on microstructure of AZ31/Al_2O_3 stir zone FSPed with threaded probe: (a) 800 rpm-2P; (b) 800 rpm-3P; (c) 800 rpm-4P; (d) 1000 rpm-2P; (e) 1000 rpm-3P; (f) 1000 rpm-4P; (g) 1200 rpm-2P; (h) 1200 rpm-3P; and (i) 1200 rpm-4P [42].

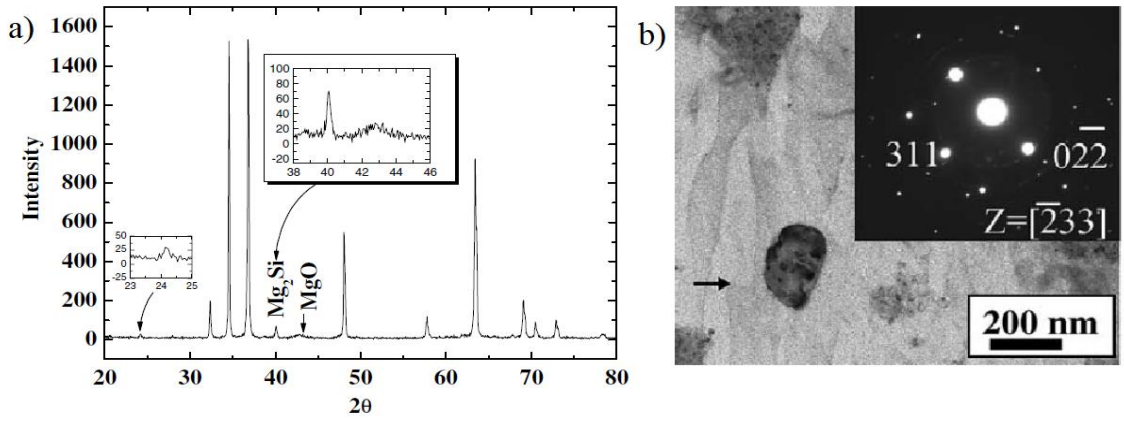

Fig. 6 a) X-ray diffraction and b) TEM/EDS results showing the presence of Mg2Si in the FSP AZ91/SiO2 composite specimens [46].

3-2- Mechanical properties evaluation of Mg-based containing ZrO_2, SiO_2, and Al_2O_3

Refinement of the microstructure was responsible for the apparent improvement in the mechanical characteristics of the generated composite. This was made possible by the hard ZrO_2 particles' fine distribution and the pinning action they had on the grain boundaries. The observed SZ microhardness values in the produced composite were contrasted with the output of an existing Hall-Petch type equation that was created to determine hardness in relation to grain size. Using FSP, Navazani et al. [31] created surface layer composites of magnesium zinc oxide. The addition of ZrO_2 particles increased the hardness and tensile strength, shown in Fig. 7 (a,b). In actuality, smaller grains increase the manufactured composite's strength and hardness by providing a stronger resistance to dislocation movement.

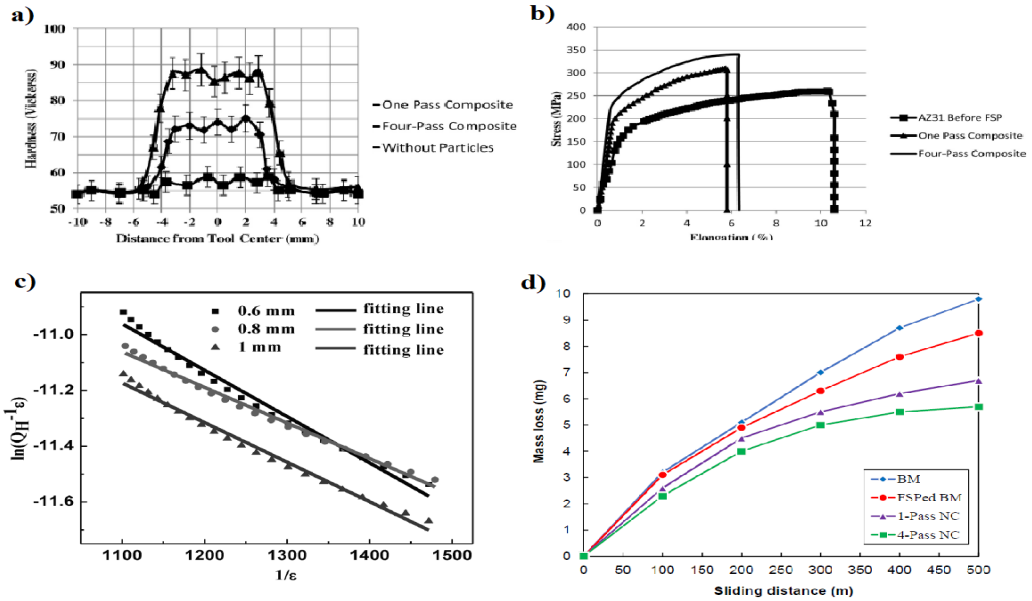

Fig. 7 (a) Hardness variations in the stir zone, (b) Stress variations before and after producing composite [23], (c) Damping-capacity dependence on the strain amplitude of ZrO2/Mg composites with different ZrO2 amounts [35] and (d) Mass loss of the samples against sliding distance [36].

The FSP of hybridized AZ31B alloy-based composites with the addition of CeO_2 and ZrO_2 powders was studied by Liu et al. [34]. Because of flaw removal and particle-aided strengthening, the tensile strength of the AZ31B Mg/(ZrO_2+CeO_2) hybrid composite surged from 172 to 228 MPa when the tool's velocity rose. Microhardness rises from 99 to 135 HV as well. Other research showed CeO_2+ZrO_2 act as great filler for strengthen Mg-based alloy [77]. The impact of incorporating ZrO_2 NPs on damping capacities was examined by Chen et al. [35]. A representative dislocation strain/damping spectrum is displayed in Fig. 7(c), which displays the damping-capacity dependency on the strain intensity of the ZrO_2/Mg composites with groove widths of (0.6, 0.8, and 1 mm). At a minimal strain intensity, the damping values Q_0^{-1} ($\varepsilon = 10^{-4}$) of the ZrO_2/Mg composites with varying ZrO_2 concentrations were 0.0111, 0.0117, and 0.0101, in that order. In overall, it is thought that an alloy has an elevated damping potential when the value is more than 0.01. The tribological performance of AZ31/ZrO_2 surface nanocomposites (NC) produced by FSP was investigated by Mazaheri et al. [36]. The inclusion of ZrO_2 NPs and raising pass number have an impact on wear resistance; however, the wear rate of the four-pass FSPed nanocomposite (4-pass NC) was approximately half of the neat AZ31 (Fig. 7(d)). Additionally, the addition of NPs and the application of FSP decreased the average friction coefficient of the AZ31 base metal. For the 4-pass NC, the average friction coefficient of the AZ31 base metal decreased from 0.5 to 0.22.

The impact of three distinct Al_2O_3 particle sizes, two distinct tool shapes, and a variety of passes in the FSP on the as-cast magnesium alloy AZ91's grain size, cluster size, microstructure, and micro-hardness were examined by Faraji et al. [43]. The findings indicate that a decrease in particle size corresponds to a boost in hardness. The triangle tool produces a harder sample compared to the square tool, and a monotonous hardness curve results from boosting the overall amount of passes (Fig. 8(a)).

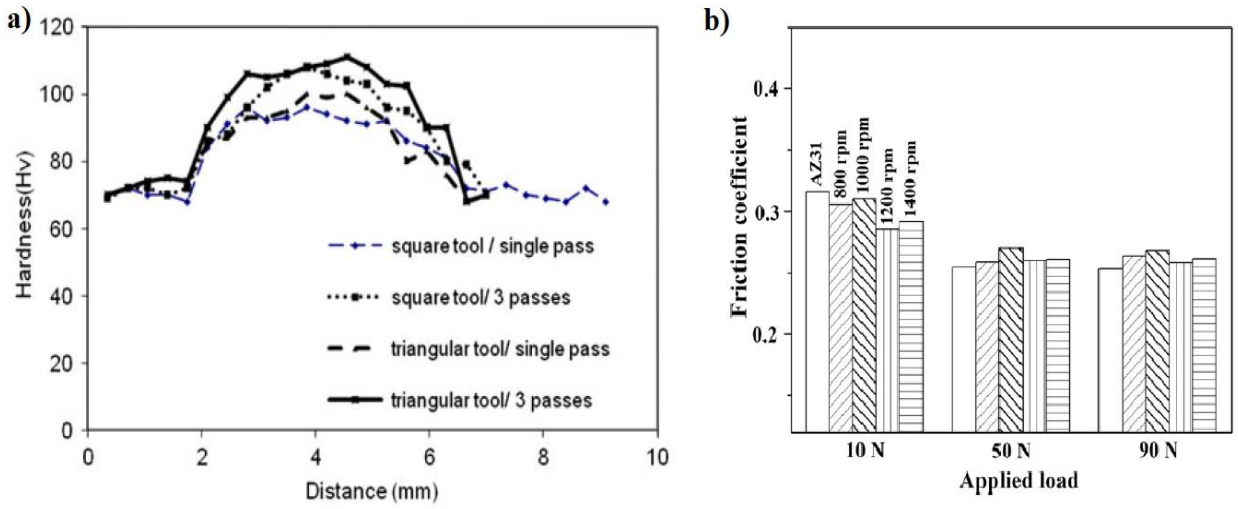

Fig. 8 (a) Effect of tool geometry and number of passes on microhardness profile in AZ91/Al2O3 composite [43], and (b) Mean friction coefficient of the as-received AZ31 alloy and AZ31/Al2O3 NC samples [41].

The wear characteristics of AZ31/Al_2O_3 magnesium matrix surface NC produced via FSP was examined by Azizieh et al. [41]. The outcomes demonstrated although while the dispersion of Al_2O_3 NPs was better, the hardness of the surface NC reduced as the velocity of rotation rose (Fig. 8(b)). Furthermore, a direct correlation between resistance to wear and the Al_2O_3 NP dispersion was discovered. Similar findings were also reported by Lu et al. [38], Asadi et al. [39], and Mostafa et al. [82]. In their study, Khayyamin et al. [49] examined the AZ91/SiO2 composite made by FSP. UTS, elongation, and microhardness of the parent metal increased when FSP was applied to the AZ91 base metal. When FSP was applied in many passes, the reinforcement's dispersion evolved into more homogeneous and UTS climbed as a result.

4- FSP with carbide ceramics reinforcement

Ceramics made with carbide have exceptional resistance to corrosion, abrasion, and high temperatures. Their primary applications include mechanical, chemical, and power engineering, microelectronics, and space engineering. They possess a high thermal and changeable electrical conductivity. The exceptional qualities of carbides can be combined into a single substance using a variety of theories and methods. The specific material is selected and developed based on its By using FSP, Bagheri et al. [58] examined the impact of process variables and vibration on the microstructure as well as mechanical properties of the AZ91/SiC surface composite. It is widely recognized that small grains form and grains are polished throughout FSP as a result of the development of DRX. A diagram of the layout is shown in Fig. 9(ii). Because the dislocations are located at low-angle grain boundaries, or low angle grain boundaries (LAGBs), the material's Gibbs free energy is reduced. Small grains develop, high angle grain boundaries (HAGBs) replace LAGBs, and the misorientation between neighboring sub-grains grows as deformation continues. Asadi et al.'s study [59] examined the impact of SiC particle size and process variables on the hardness and microstructure of an FSP-fabricated AZ91/SiC composite film. Through the elimination of eutectic β-phase precipitated near grain boundaries, FSP creates a homogenous microstructure. Additionally, homogenous microstructure and grain refinement composite were generated by FSP on SiC-magnesium and SiC-magnesium alloys production technology as well as usage demands. In the category of carbide ceramics, silicon carbide is the most significant component, next to titanium carbide and boron. The SiC, B4C, and TiC reinforced magnesium matrix composites were effective in attaining grain modification, excellent hardness, and wear performance.

4-1- Microstructure evaluation of Mg-based containing SiC, B4C, and TiC

FSP was utilized by Peng et al. [53] to create the AZ31/SiC magnesium composite. Using multipass FSP, SiC particles with an average size of 60 nm and 1 μm were added to the AZ31 Mg alloy. Because of the extreme plastic deformation throughout FSP, the grains underwent substantial refinement following the process. The specimen with SiC particles added had a somewhat lower grain size compared the specimen without them. SiC particles produced lower grain sizes and enhanced the DRX throughout FSP. The microstructure in the SZ and TMAZ was investigated using an optical microscope with the aim to provide light on the microstructure progression throughout FSP, as seen in 9 (i). by Iwaszko et al. [50], Deepan et al. [56], and Ram et al. [55]. By using FSP, Singh et al. [61] created a Mg/TiC composite.

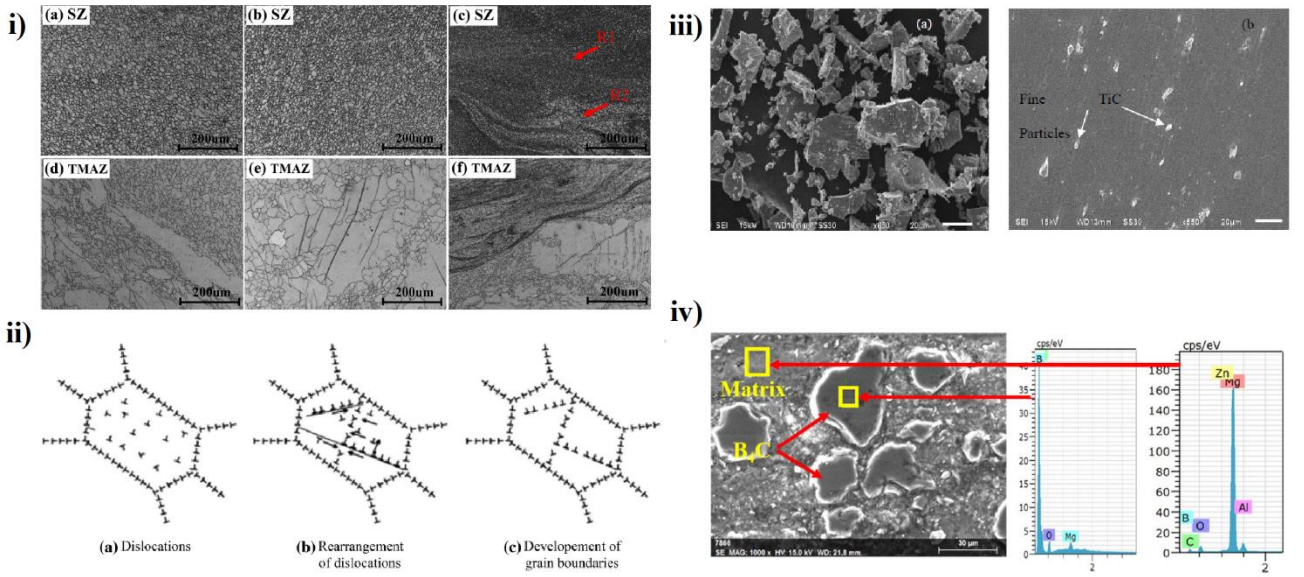

Fig. 9 i) Microstructure of the samples a, d without SiC particles and with b, e 60 nm and c, f 1 µm SiC particles in the SZ and TMAZ [53], ii) Illustration of steps for grain refinement during FSP [58], iii) SEM micrograph of (a) TiC powder and (b) Surface fabricated surface composite [61], and iv) SEM image and corresponding EDS analysis of AZ91/B_4Csurface composite [66].

The SEM micrograph of the manufactured surface composite is displayed in Fig. 9(b), and the SEM image of the TiC powder employed in the investigation is represented in Fig. 9(iii). Additionally, the image depicts the refining of pure magnesium substrate metal grains. Comparable results have been documented by Sagar et al. [64, 65, 89].

The sliding wear performance of AZ91/B4C surface composites generated via FSP was examined by Patle et al. [66]. The SEM image from the stir zone of the FSPed AZ91/B4C sample is displayed in Fig. 9(iv). It is evident how the B4C particles are dispersed across the stir zone. The elemental makeup of the matrix and the scattered B4C particles are displayed in the accompanying EDS analysis. The stir zone's B4C particles were evenly distributed, according to SEM examination. The orderly arrangement of particles is a key factor in improving the manufactured surface composite's hardness and wear performance. Phase transition in magnesium alloy is a recognized occurrence because of the high heat generated during FSP. Following FSP in the AZ91Mg alloy, dissolution of intermetallic phases (β phase, $Mg_{17}Al_{12}$) in the solid solution grains (α phase) was noted. The mechanical characteristics of the composites is influenced by the inclusion of secondary phase particles and the reduction of intermetallic phases alongside grain refinement. [67, 90].

4-2- Mechanical properties evaluation of Mg-based containing SiC, B4C, and TiC

According to the investigations, Mg-SiC composites produced using FSP have improved wear performance, fatigue resistance, tensile strength, hardness, ductility, and defect elimination. The finely recrystallized microstructure, finely sized reinforcement, porosity-free area, and homogeneous distribution of SiC particles inside the matrix can all be credited with a boost of the mechanical characteristics. SiC NPs strengthened the matrix in two different ways. In the first process, stresses were transferred from the matrix to the NPs. The

second process involved the induction of dislocations surrounding the NPs by the differential in cooling between the matrix and the NPs, but the NPs themselves inhibited dislocation. Furthermore, according to the Hall-Petch connection, microhardness rises and grain size diminishes in tandem. Therefore, the primary cause of the treated samples' better mechanical characteristics over the as-received samples is their smaller grain size and the existence of second-phase particles. The volume proportion of grain borders increases with decreasing grain size. Dislocations are impeded and strength is increased by grain boundaries and second-phase particles [51, 52, 54, 57, 59, 60, 83, 84, 85, 86].

The microstructural modification provided by the intense plastic deformation that happened throughout FSP and the inclusion of TiC particles is what Singh et al. [61] found to be responsible for a boost in the ultimate strength and yield strength of pure magnesium. Therefore, by raising the tensile strength and lessening the elasticity of the base material magnesium, the inclusion of hard particles of TiC serves to adjust the material's mechanical characteristics (Fig. 10)). The modulus of the treated composite is additionally improved by the grain refinement provided by the TiC-particles in the FSP manufactured surface composite.

The impact of tool rotation velocity on the tribological properties of the magnesium-based AZ61A/ TiC composite was investigated by Sagar et al. [64] using FSP. When opposed to base metal, they revealed a reduced wear rate, which might be explained by higher hardness levels. The wear characteristics of B4C strengthened AZ91 matrix composite, which was manufactured via FSP, was examined by Singh et al. [67]. They found that the average hardness and wear resistance rose in a direct relationship to a boost in particle size, meaning that their values rise with increasing particle size.

5- FSP with carbon base reinforcements

Metal matrix composites' mechanical qualities are enhanced with the introduction of carbon reinforcements. The hardness, tensile strength, elastic modulus, and other mechanical characteristics of metal matrices are greatly enhanced by the addition of these kinds of

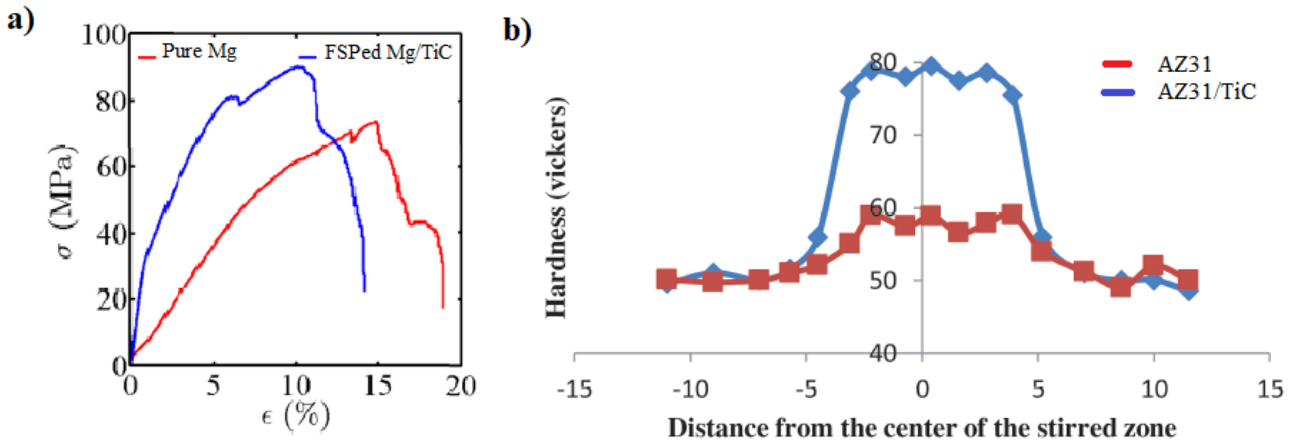

Fig. 10 a) Stress (σ) versus strain (ϵ) plot obtained from the tensile testing of pure Mg and Mg+TiC composite fabricated by FSP [61], and b) Hardness Variation of AZ31 alloy and AZ31/TiC composite [62].

fillers. Studies have been conducted on graphene-magnesium composites, carbon fiber (CF), and carbon nanotubes (CNTs) using FSP.

5-1- Microstructure evaluation of Mg-based containing CNTs, CF, and Gr

The mechanisms of CNT/Mg-6Zn composites' toughening and strengthening were investigated by Huang et al. [70] using FSP. As shown in Fig. 11(i), the entire manufacturing procedure consists of the pre-dispersion of CNTs, stirring casting, and FSP thereafter. They showed that the singly distributed CNTs created a compact bonding with the matrix, which improved the Mg-6Zn matrix's mechanical characteristics and refined its grain. The Orowan looping mechanisms, load transfer, and grain refining provide the basis for the strengthening effects.

CNTs/Mg composites were made by Liang et al. [71] through the use of FSP with ultrasonic aided extrusion. Fig. 11 shows a TEM image at the interface where the Mg matrix and CNTs existed. Fig. 11(a) indicates that a needle-like phase is clearly distinct from the magnesium matrix, as indicated by a white arrow. The diffraction pattern of the chosen region around Fig. 11 ii(b) as presented in Fig. 11ii(c) indicates the existence of Al_2MgC_2 within the region. These sources' Al_2MgC_2 shapes are comparable to the one created in this study. It is consequently possible to identify the unidentified needle-like phase as Al_2MgC_2. Compared to Al_4C_3, the crystal structure of Al_2MgC_2 is substantially more similar to that of Mg. From the perspective of crystal structure, Al_2MgC_2 forms more readily compared to Al_4C_3. An inverse FFT image of the magnesium matrix is displayed in Fig. 11(c), in which the parallel layers readily apparent the crystalline characteristics. Additionally, this image has a number of flaws, including edge dislocations. The

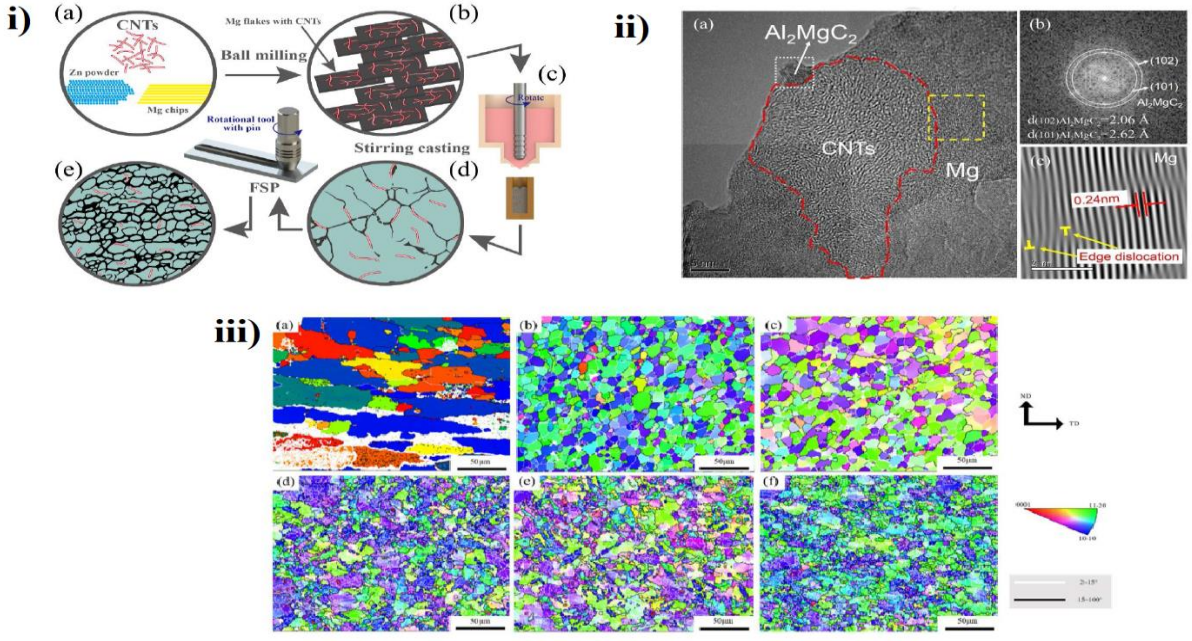

Fig. 11 i) Schematics for the fabrication procedures of the CNTs/Mg-6Zn composites: (a) the as-received materials, (b) the deposited CNTs with Mg chips by pre-treatments, (c) stirring casting, (d) microstructure morphology and CNTs distribution for the as-cast [70], and (e) the FSPed composites, ii) (a) High resolution TEM micrograph of Mg NC, (b) A digital SAEDP using a fast Fourier transform (FFT) of the area inside the white box in (a). (c) Inverse FFT image of the area inside the yellow box in (a) [71], The yellow T indicates the position and orientation of dislocation and iii) e EBSD IPF maps of different samples: (a) BM; (b) FSP sample; (c) AZ31/GNP composites; (d) FSP +50% rolling; (e) FSP þ40% rolling + GNP; (f) FSP +50% rolling + GNP [75].

presence of edge dislocations at the interface between carbon nanotubes and magnesium is evident in the inset with enhanced resolution, and this is the primary cause of the improved mechanical characteristics.

Through the use of FSP and rolling, Zhang et al. [75] manufactured magnesium composites containing AZ31 and graphene nanoparticulates (GNP). The outcomes demonstrated that the extreme plastic deformation properties of FSP are responsible for the second phase's homogeneity and grain refinement, which in turn accounts for the increased performance. Strength is additionally derived by the reinforcing of GNP and the multiplication of dislocations originating from rolling deformation. The outcomes confirm that adding strengthening particles by using FSP as a step prior rolling is potentially a successful strategy. However, the enhanced microstructure brought about by the extreme plastic deformation of FSP is advantageous for additional rolling. Samples' grain size distribution maps are displayed in Fig. 11(iii).

5-2- Mechanical properties evaluation of Mg-based containing CNTs, CF, and Gr

The microstructure and mechanical characteristics of AZ31/SiC and AZ31/CNT composites made by FSP were examined by Alavi Nia et al. [72]. Grain generated by FSP was more homogeneous and smaller. As the number of passes rose, the homogeneity improved and the grain size dropped. The mechanical characteristics were enhanced by the reduction in grain size. The addition of CNTs stabilized the grain size and improved the homogeneity of the structure. Fig. 12(a) displays the stress-strain curves for the base material with one, four, and eight passes of FSP without reinforcing particles as well as with four, eight, and sixteen percent (v/v) SiC NPs and CNTs. Similar outcomes were also reported by Kim et al. [68].

Additionally, the hybrid application of CNT-Graphene fillers improved the magnesium matrix composites' mechanical characteristics [68, 69]. Through the use of FSP, Afrinaldi et al. [76] created a carbon fiber strengthened AZ91 magnesium alloy composite and examined its fatigue characteristics. The S-N curves of the MMC manufactured with the 3-fat pin tool, the as-cast material, and the FSPed ones without CFs6) are displayed in Fig. 12(b). The as-cast samples' fatigue strengths show significant scatter, but they also tend to show a distinct knee at about 105 cycles, which results in a fatigue strength of 40 MPa at 107 cycles (referred to as the fatigue limit). However, when compared to the as-cast samples, the fatigue strengths of the FSPed samples without CFs are significantly higher (fatigue limit 80 MPa). Nonetheless, the MMC samples' fatigue strengths are inferior to those of the FSPed samples without CFs and comparable to those of the as-cast samples, particularly at stress levels below 80 MPa. Fatigue cracks that started at the CF aggregation. It suggests that the agglomeration of CFs reduced the barrier to fatigue crackformation, which is why the fatigue strengths of the FSPed samples with CFs were lower compared to those without CFs. According to Zhang et al. [75], the primary processes of strengthening consist of precipitation strengthening, dislocation strengthening, grain refinement strengthening (according to the Hall-Petch equation), and consolidating phase strengthening. Particles of GNP is responsible for the enhanced strength of MMCs are as follows: (a) Orowan looping; (b) reinforcement phase load transfer; and (c) coefficient of thermal expansions (CTE) mismatch mechanism. All of the samples' engineering stress-strain curves were shown in Fig. 12(c, d). Other investigations

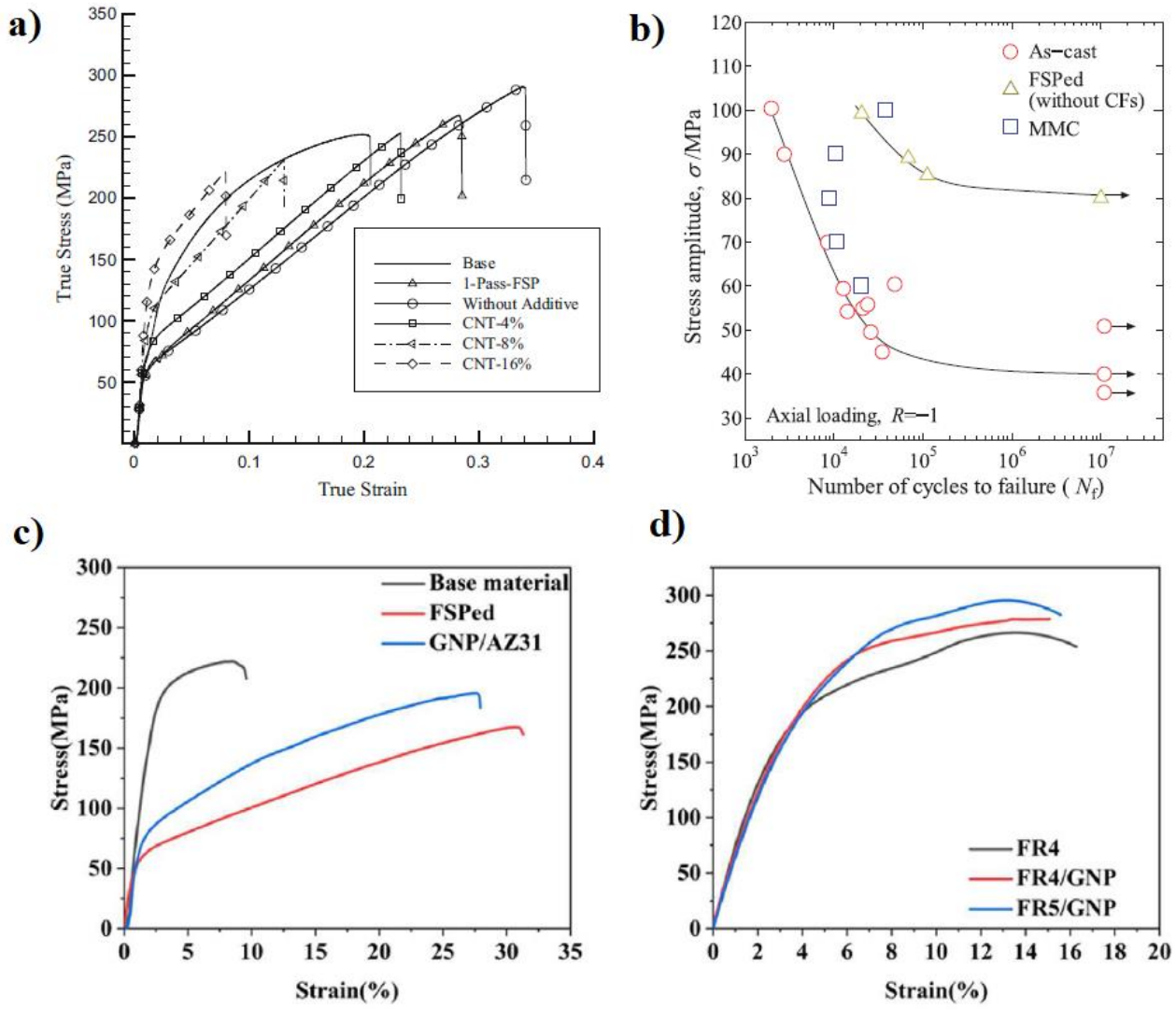

Fig. 12 a) Stress–strain curves of the raw material with one pass FSP process, four passes FSP process without reinforcing particles and with 4, 8 and 16 percentages of CNT [72], b) S-N diagram of carbon fiber reinforced AZ91 magnesium alloy composite [76], c) Room temperature tensile engineering stress-strain curves of BM, sample F and F/GNP and (b) sample FR5, FR4/GNP and FR5/GNP [75].

regarding the incorporation of GNP as filler for magnesium alloys exhibited similar findings [91, 92].

6- Conclusion

This review paper covers the fundamentals of microstructure conversion and how adding ceramic reinforcement particles during the FSP of Mg alloys can improve mechanical properties by adding SiC, SiO_2, Al_2O_3, B_4C, TiC, and ZrO_2. Uniform dispersion, minimal dislocation densities, and the absence of casting- related or porosity-related flaws are the characteristics of the FSPed microstructure. This well-characterized microstructure enhances the mechanical, corrosion, and tribological characteristics of magnesium alloys. By performing additional processing passes, the agglomeration and homogeneous dispersion of reinforcing particles can be further enhanced. Reinforcing particles boost the tensile strength, wear resistance, and surface hardness of Mg alloys. The two primary mechanisms responsible for

the mechanical characteristics enhancement of Mg-based SMMCs are dispersion strengthening and fine-grained strengthening. When reinforcing particles are added to the metal matrix, particle-stimulated nucleation favors the formation of grains during recrystallization. The evenly distributed small particles may hinder grain formation throughout the DRX procedure, based on the grain refinement strengthening. This happens as a consequence of the microstructure being significantly refined by the pinning effect on the grain boundaries. It is important to bear in mind that adding more reinforcing particles could cause the agglomeration phenomena to become more noticeable, which would have an impact on the functionality of composite materials. There aren't many studies that discuss solutions for this issue. Therefore, future studies should focus on ways to remove porosity and agglomeration while uniformly redistributing multi-reinforced particles.

References

[1] Clyne, T. W., & Hull, D. (2019). *An introduction to composite materials*. Cambridge university press.

[2] Mishra, R. S., & Ma, Z. Y. (2005). Friction stir welding and processing. *Materials science and engineering: R: reports*, *50*(1-2), 1-78.

[3] Padhy, G. K., Wu, C. S., & Gao, S. (2018). Friction stir based welding and processing technologies-processes, parameters, microstructures and applications: A review. *Journal of Materials Science & Technology*, *34*(1), 1-38.

[4] Mishra, R. S., Mahoney, M. W., McFadden, S. X., Mara, N. A., & Mukherjee, A. K. (1999). High strain rate superplasticity in a friction stir processed 7075 Al alloy. *Scripta materialia*, *42*(2), 163-168.

[5] Badkoobeh, F., Mostaan, H., Rafiei, M., Bakhsheshi-Rad, H. R., & Berto, F. (2021). Friction stir welding/processing of Mg-based alloys: a critical review on advancements and challenges. *Materials*, *14*(21), 6726.

[6] Gotawala, N., Kumar, A., Mishra, S., & Shrivastava, A. (2021). Microstructure and texture evolution of complete Mg-3Al-0.2 Ce alloy blanks upon multi-pass friction stir processing with spiral strategy. Materials Today Communications, 26, 101850.

[7] Zykova, A. P., Tarasov, S. Y., Chumaevskiy, A. V., & Kolubaev, E. A. (2020). A review of friction stir processing of structural metallic materials: Process, properties, and methods. Metals, 10(6), 772.

[8] Ma, Z. Y. (2008). Friction stir processing technology: a review. *Metallurgical and materials Transactions A*, *39*, 642-658.

[9] Butola, R., Pandit, D., Pratap, C., & Chandra, P. (2022). Two decades of friction stir processing–a review of advancements in composite fabrication. Journal of Adhesion Science and Technology, 36(8), 795-832.

[10] Tamadon, A., Pons, D. J., Sued, K., & Clucas, D. (2017). Development of metallographic etchants for the microstructure evolution of A6082-T6 BFSW welds. Metals, 7(10), 423.

[11] Li, K., Liu, X., & Zhao, Y. (2019). Research status and prospect of friction stir processing technology. *Coatings*, *9*(2), 129.

[12] Chang, C. I., Lee, C. J., & Huang, J. C. (2004). Relationship between grain size and Zener–Holloman parameter during friction stir processing in AZ31 Mg alloys. *Scripta materialia*, *51*(6), 509-514.

[13] Chen, F. X., Li, H. J., Guo, J. Q., Yang, Y. S., & Xu, G. Z. (2007, July). Study of the superplasticity of copper alloys used for solid cages. In *Materials science forum* (Vol. 551, pp. 79-83). Trans Tech Publications Ltd.

[14] Boissière, R., Blandin, J. J., & Salvo, L. (2010). Large deformability of wrought magnesium alloys: is superplasticity needed?. *Key Engineering Materials*, *433*, 267-272.

[15] Sadeghi-Ghoghery, M., Kasiri-Asgarani, M., & Amini, K. (2017). Friction stir welding of dissimilar joints between commercially pure titanium alloy and 7075 aluminium alloy. *Transactions of FAMENA*, *41*(1), 81-90.

[16] Gogheri, M. S., Kasiri-Asgarani, M., Bakhsheshi-Rad, H. R., Ghayour, H., & Rafiei, M. (2020). Mechanical properties, corrosion behavior and biocompatibility of orthopedic pure titanium− magnesium alloy screw prepared by friction welding. *Transactions of Nonferrous Metals Society of China*, *30*(11), 2952-2966.

[17] Gogheri, M. S., Kasiri-Asgarani, M., Bakhsheshi-Rad, H. R., Ghayour, H., Rafiei, M., Mostafa, A., & Berto, F. (2022). Friction welding of pure titanium-AZ31 magnesium alloy: Characterization and simulation. *Engineering Failure Analysis*, *131*, 105799.

[18] *Babu*, S. R., Kumar, V. S., Karunamoorthy, L., & Reddy, G. M. (2014). Investigation on the effect of friction stir processing on the superplastic forming of AZ31B alloy. *Materials & Design*, *53*, 338-348.

[19] Kaibyshev, R., Sitdikov, O., & Olenyov, S. (2002). Ultrafine Grain Formation During Equal Channel Angular Extrusion in an Al-Mg-Sc Alloy. *Ultrafine grained materials II*, 65-74.

[20] Mirzadeh, H. (2021). High strain rate superplasticity via friction stir processing (FSP): A review. *Materials Science and Engineering: A*, *819*, 141499.

[21] Alizadeh, R., Mahmudi, R., Ngan, A. H. W., Huang, Y., & Langdon, T. G. (2016). Superplasticity of a nano-grained Mg–Gd–Y–Zr alloy processed by high-pressure torsion. *Materials Science and Engineering: A*, *651*, 786-794.

[22] Kandalam, S., Sabat, R. K., Bibhanshu, N., Avadhani, G. S., Kumar, S., & Suwas, S. (2017). Superplasticity in high temperature magnesium alloy WE43. *Materials Science and Engineering: A*, *687*, 85-92.

[23] Iwaszko, J., & Sajed, M. (2021). Technological aspects of producing surface composites by friction stir processing—A review. *Journal of Composites Science*, *5*(12), 323.

[24] Wu, B., Ibrahim, M. Z., Raja, S., Yusof, F., Muhamad, M. R. B., Huang, R., ... & Kamangar, S. (2022). The influence of reinforcement particles friction stir processing on microstructure, mechanical properties, tribological and corrosion behaviors: a review. *Journal of Materials Research and Technology*, *20*, 1940-1975.

[25] Saberi, A., Bakhsheshi-Rad, H. R., Karamian, E., Kasiri-Asgarani, M., & Ghomi, H. (2020). Magnesium-graphene nano-platelet composites: Corrosion behavior, mechanical and biological properties. *Journal of Alloys and Compounds*, *821*, 153379.

[26] Razzaghi, M., Kasiri-Asgarani, M., Bakhsheshi-Rad, H. R., & Ghayour, H. (2020). Microstructure, mechanical properties, and in-vitro biocompatibility of nano-NiTi reinforced Mg–3Zn-0.5 Ag alloy: Prepared by mechanical alloying for implant applications. *Composites Part B: Engineering*, *190*, 107947.

[27] Razzaghi, M., Kasiri-Asgarani, M., Bakhsheshi-Rad, H. R., & Ghayour, H. (2021). In vitro bioactivity and corrosion of PLGA/hardystonite composite-coated magnesium-based nanocomposite for implant applications. *International Journal of Minerals, Metallurgy and Materials*, *28*(1), 168-178.

[28] Vatan, H. N., Kahrizsangi, R. E., & Asgarani, M. K. (2016). Growth, corrosion and wear resistance of SiC nanoparticles embedded MAO coatings on AZ31B magnesium alloy. *Protection of Metals and Physical Chemistry of Surfaces*, *52*(5), 859-868.

[29] Qiao, K., Zhang, T., Wang, K., Yuan, S., Wang, L., Chen, S., ... & Wang, W. (2022). Effect of multi-pass friction stir processing on the microstructure evolution and corrosion behavior of ZrO2/AZ31 magnesium matrix composite. *Journal of Materials Research and Technology*, *18*, 1166-1179.

[30] Vaira Vignesh, R., Padmanaban, R., Govindaraju, M., & Suganya Priyadharshini, G. (2019). Investigations on the corrosion behaviour and biocompatibility of magnesium alloy surface composites AZ91D-ZrO2 fabricated by friction stir processing. *Transactions of the IMF*, *97*(5), 261-270.

[31] Navazani, M., & Dehghani, K. (2016). Fabrication of Mg-ZrO2 surface layer composites by friction stir processing. *Journal of Materials Processing Technology*, *229*, 439-449.

[32] Zang, Q., Li, X., Chen, H., Zhang, J., Wang, L., Chen, S., & Lu, S. (2020). Microstructure and *mechanical* properties of AZ31/ZrO2 composites prepared by friction stir processing with high rotation speed. *Frontiers in Materials*, *7*, 278.

[33] Qiao, K., Zhang, T., Wang, K., Yuan, S., Zhang, S., Wang, L., & Wang, W. (2021). Mg/ZrO2 metal matrix *nanocomposites* fabricated by friction stir processing: microstructure, mechanical properties, and corrosion behavior. *Frontiers in Bioengineering and Biotechnology*, *9*, 605171.

[34] Liu, S., Paidar, M., Ojo, O. O., Poková, M. Š., Mehrez, S., Zain, A. M., ... & Wang, J. (2023). Friction stir processing of hybridized AZ31B magnesium alloy-based composites by adding CeO2 and ZrO2powders: mechanical, wear, and

corrosion behaviors. *Journal of Materials Research and Technology*, *24*, 1949-1972.

[35] POSTOPKOM, V. T. (2019). Effect of zro2 additions on fabrication of zro2/mg composites via friction-stir processing. *Mater Tehnologije*, *53*(2), 193-197.

[36] Mazaheri, Y., Jalilvand, M. M., Heidarpour, A., & Jahani, A. R. (2020). Tribological behavior of AZ31/ZrO2 surface nanocomposites developed by friction stir processing. *Tribology International*, *143*, 106062.

[37] Li, Y., Ojo, O. O., Salman, S., Paidar, M., Refaai, M. R. A., Zain, A. M., ... & Xin, D. (2023). Fabrication of the novel hybridized AZ31B Mg/CeO2+ ZrO2 composites via multiple pass friction stir processing. Journal of Materials Research and Technology, 24, 9984-10004.

[38] Lu, D., Jiang, Y., & Zhou, R. (2013). Wear performance of nano-Al2O3 particles and CNTs reinforced magnesium matrix composites by friction stir processing. Wear, 305(1-2), 286-290.

[39] Ahmadkhaniha, D., Sohi, M. H., Salehi, A., & Tahavvori, R. (2016). Formations of AZ91/Al2O3 nano-composite layer by friction stir processing. Journal of *Magnesium and Alloys*, *4*(4), 314-318.

[40] Asadi, P., Faraji, G., Masoumi, A., & Besharati Givi, M. K. (2011). Experimental investigation of magnesium-base nanocomposite produced by friction stir processing: effects of particle types and number of friction stir processing passes. *Metallurgical and Materials Transactions A*, *42*, 2820-2832.

[41] Azizieh, M., Larki, A. N., Tahmasebi, M., Bavi, M., Alizadeh, E., & Kim, H. S. (2018). Wear behavior of AZ31/Al 2 O 3 magnesium matrix surface nanocomposite fabricated via friction stir processing. *Journal of Materials Engineering and Performance*, *27*, *2010-2017*.

[42] Azizieh, M., Kokabi, A. H., & Abachi, P. (2011). Effect of rotational speed and probe profile on microstructure and hardness of AZ31/Al2O3 nanocomposites fabricated by friction stir processing. Materials & Design, *32*(4), 2034-2041.

[43] Faraji, G., *Dastani*, O., & Mousavi, S. A. A. A. (2011). Effect of process parameters on microstructure and micro-hardness of AZ91/Al 2 O 3 surface composite produced by FSP. *Journal of Materials Engineering and Performance*, *20*, 1583-1590.

[44] Sharifitabar, M., Kashefi, M., & Khorshahian, S. (2016). Effect of friction stir processing pass sequence on properties of Mg–ZrSiO4–Al2O3 surface hybrid micro/nano-*composites*. *Materials & Design*, *108*, 1-7.

[45] Rezaeian-Delouei, M., Abdollah-Pour, H., Tajally, M., & Mousavizade, S. M. (2020). An investigation of microstructure, *wear* and corrosion resistance of AZ31B–SiO2–graphite hybrid surface composite produced by friction stir processing. *Materials Research Express*, *6*(12), 1250a7.

[46] Lee, C. J., Huang, J. C., & Hsieh, P. J. (2006). Mg based nano-composites fabricated by friction stir processing. Scripta Materialia, 54(7), 1415-1420.

[47] Chang, C. I., Wang, Y. N., Pei, H. R., Lee, C. J., Du, X. H., & Huang, J. C. (2007). Microstructure and mechanical properties of nano-ZrO2 and nano-SiO2 particulate reinforced AZ31-Mg based composites fabricated by friction stir processing. Key Engineering Materials, 351, 114-119.

[48] CI, C., YN, W., HR, P., & JC, H. (2006). On the hardening of friction stir processed Mg-AZ31 based composites with 5–20% nano-ZrO2 and nano-SiO2 particles. Materials transactions, 47(12), 2942-2949.

[49] Khayyamin, D., Mostafapour, A., & Keshmiri, R. (2013). The effect of process parameters on microstructural characteristics of AZ91/SiO2 composite fabricated by FSP. *Materials Science and Engineering: A*, *559*, 217-221.

[50] Iwaszko, J., Kudła, K., & Fila, K. (2016). Friction stir processing of the AZ91 magnesium alloy with SiC particles. *Archives of Materials Science and Engineering*, *77*(2), 85-92.

[51] Rajmohan, T., Prasad, K. G., Jeyavignesh, S., Kamesh, K., Karthick, S., & Duraimurugan, S. (2018, July). Studies on friction stir processing parameters on microstructure and micro hardness of Silicon carbide (SiC) particulate reinforced Magnesium (Mg) surface composites. In *IOP Conference Series: Materials Science and Engineering* (Vol. 390, No. 1, p. 012013). IOP Publishing.

[52] Ram, B., Deepak, D., & Bala, N. (2019). Microstructural refinement and enhancement in mechanical properties of magnesium/SiC as-cast

composites via friction stir processing route. *Transactions of the Indian Institute of Metals*, *72*, 1313-1321.

[53] Peng, J., Zhang, Z., Guo, P., Huang, J. A., Zhou, W., & Wu, Y. (2020). Microstructure and tensile properties of SiC particles reinforced AZ31 magnesium alloys prepared by multi-pass friction stir processing. *Transactions of the Indian Institute of Metals*, *73*(4), 1093-1099.

[54] Naser, A. Z., & Darras, B. M. (2017). Experimental investigation of Mg/SiC composite fabrication via friction stir processing. *The International Journal of Advanced Manufacturing Technology*, *91*, 781-790.

[55] Ram, B., Deepak, D., & Bala, N. (2018). Role of friction stir processing in improving wear behavior of Mg/SiC composites produced by stir casting route. *Materials Research Express*, *6*(2), 026577.

[56] Deepan, M., Pandey, C., Saini, N., Mahapatra, M. M., & Mulik, R. S. (2017). Estimation of strength and wear properties of Mg/SiC nanocomposite fabricated through FSP route. *Journal of the Brazilian Society of Mechanical Sciences and Engineering*, *39*, 4613-4622.

[57] Morisada, Y., Fujii, H., Nagaoka, T., & Fukusumi, M. (2006). Effect of friction stir processing with SiC particles on microstructure and hardness of AZ31. *Materials Science and Engineering: A*, *433*(1-2), 50-54.

[58] Bagheri, B., & Abbasi, M. (2020). Development of AZ91/SiC surface composite by FSP: effect of vibration and process parameters on microstructure and mechanical characteristics. *Advances in Manufacturing*, *8*(1), 82-96.

[59] Asadi, P., Givi, M. B., Abrinia, K., Taherishargh, M., & Salekrostam, R. (2011). Effects of SiC particle size and process parameters on the microstructure and hardness of AZ91/SiC composite layer fabricated by FSP. *Journal of materials engineering and performance*, *20*, 1554-1562.

[60] Bagheri, B., Abbasi, M., Abdollahzadeh, A., & Mirsalehi, S. E. (2020). Effect of second-phase particle size and presence of vibration on AZ91/SiC surface composite layer produced by FSP. *Transactions of Nonferrous Metals Society of China*, *30*(4), 905-916.

[61] Singh, B., Singh, J., & Joshi, R. S. (2022). Effect of tic reinforcement on wear resistance of magnesium matrix composite by Fsp. *Archives of Metallurgy and Materials*, 293-302.

[62] Navazani, M., & Dehghani, K. (2015). Investigation of microstructure and hardness of Mg/TiC surface composite fabricated by friction stir processing (FSP). *Procedia Materials Science*, *11*, 509-514.

[63] Balakrishnan, M., Dinaharan, I., Palanivel, R., & Sivaprakasam, R. (2015). Synthesize of AZ31/TiC magnesium matrix composites using friction stir processing. *Journal of Magnesium and Alloys*, *3*(1), 76-78.

[64] Sagar, P., & Handa, A. (2020). Role of tool rotational speed on the tribological characteristics of magnesium based az61a/tic composite developed via friction stir processing route. *Journal of Achievements in Materials and Manufacturing Engineering*, *101*(2), 60-75.

[65] Sagar, P., & Handa, A. (2021). Selection of tool transverse speed considering trial run experimentations for AZ61/Tic composite developed via friction stir processing using triangular tool. *Materials Today: Proceedings*, *38*, 198-203.

[66] Patle, H., Sunil, B. R., & Dumpala, R. (2020). Sliding wear behavior of AZ91/B4C surface composites produced by friction stir processing. *Materials Research Express*, *7*(1), 016586.

[67] Singh, N., Singh, J., Singh, B., & Singh, N. (2018). Wear behavior of B4C reinforced AZ91 matrix composite fabricated by FSP. *Materials Today: Proceedings*, *5*(9), 19976-19984.

[68] Byeon, J. W., Lee, S. M., Kim, J. Y., Hwang, J. W., Kim, H. Y., & Jung, W. S. (2017). Fabrication of AZ31/CNT surface nano-composite by double-pass friction stir processing. *Archives of Metallurgy and Materials*..

[69] bin Ariffin, M. A., bin Muhamad, M. R., Raja, S., Jamaludin, M. F., Yusof, F., Suga, T., ... & Fujii, H. (2022). Friction stir alloying of AZ61 and mild steel with Cu-CNT additive. *Journal of Materials Research and Technology*, *21*, 2400-2415.

[70] Huang, Y., Li, J., Wan, L., Meng, X., & Xie, Y. (2018). Strengthening and toughening mechanisms of CNTs/Mg-6Zn composites via friction stir processing. *Materials Science and Engineering: A*, *732*, 205-211.

[71] Liang, J., Li, H., Qi, L., Tian, W., Li, X., Chao, X., & Wei, J. (2017). Fabrication and mechanical properties of CNTs/Mg composites prepared by combining friction stir processing and ultrasonic assisted extrusion. *Journal of Alloys and Compounds*, *728*, 282-288.

[72] Alavi Nia, A., & Nourbakhsh, S. H. (2016). Microstructure and mechanical properties of AZ31/SiC and AZ31/CNT composites produced by friction stir processing. *Transactions of the Indian Institute of Metals*, *69*(7), 1435-1442.

[73] Sharma, S., Handa, A., Singh, S. S., & Verma, D. (2019). Influence of tool rotation speeds on mechanical and morphological properties of friction stir processed nano hybrid composite of MWCNT-Graphene-AZ31 magnesium. *Journal of Magnesium and Alloys*, *7*(3), 487-500.

[74] Sharma, S., Handa, A., Singh, S. S., & Verma, D. (2019). Synthesis of a novel hybrid nanocomposite of AZ31Mg-Graphene-MWCNT by multi-pass friction stir processing and evaluation of mechanical properties. *Materials Research Express*, *6*(12), 126531.

[75] Zhang, M., Yang, K., Wei, G., Xie, W., Yang, Y., Li, B., ... & Yang, Q. (2023). AZ31/GNP magnesium composites with excellent comprehensive mechanical properties prepared by friction stir processing and rolling. *Journal of Materials Research and Technology*, *25*, 3078-3092.

[76] Afrinaldi, A., Kakiuchi, T., Nakagawa, S., Moritomi, H., Kumabe, K., Nakai, A., ... & Uematsu, Y. (2018). Fabrication of recycled carbon fiber reinforced magnesium alloy composite by friction stir processing using 3-flat pin tool and its fatigue properties. *Materials Transactions*, *59*(3), 475-481.

[77] Li, H., Paidar, M., Ojo, O. O., Vignesh, R. V., Iswandi, I., Mehrez, S., ... & Mohanavel, V. (2023). Effect of tool profile on wear and mechanical behaviors of CeO2 and ZrO2-reinforced hybrid magnesium matrix composite developed via FSP technique. *Journal of Manufacturing Processes*, *94*, 297-315.

[78] Zhang, M., Paidar, M., Šlapáková, M., Abdullaev, S., Refaai, M. R. A., Zain, A. M., & Vignesh, R. V. (2023). Achieving high mechanical and wear properties in the AZ31/(CeO2+ ZrO2) p surface composite using friction stir processing: Application of vibration. *Vacuum*, *218*, 112654.

[79] Ma, W., Ojo, O. O., Paidar, M., Mehrez, S., Zain, A. M., Kulandaivel, A., ... & Kannan, S. (2023). Improving the wear resistance and mechanical properties of hybridized AZ80 Mg/CeO2+ ZrO2 surface composite by friction stir processing: Effect of pin geometry. *Vacuum*, *212*, 111980.

[80] Faraji, G., Dastani, O., & Mousavi, S. A. (2011). Microstructures and mechanical properties of Al2O3/AZ91 surface nanocomposite layer produced by friction stir processing. *Proceedings of the Institution of Mechanical Engineers, Part B: Journal of Engineering Manufacture*, *225*(8), 1331-1345.

[81] Azizieh, M., Kim, H. S., Kokabi, A. H., Abachi, P., & Shahraki, B. K. (2011). Fabrication of AZ31/Al2O3 nanocomposites by friction stir processing. *Reviews on Advanced Materials Science*, *28*(1), 85-89.

[82] Dadaei, M., Omidvar, H., Bagheri, B., Jahazi, M., & Abbasi, M. (2014). The effect of SiC/Al2O3 particles used during FSP on mechanical properties of AZ91 magnesium alloy. *International Journal of Materials Research*, *105*(4), 369-374.

[83] Awasthi, S., Gupta, P., Pachuri, P., & Tyagi, M. (2022). Optimization of magnesium ZK60A/SiC/B4C hybrid composite fabricated by friction stir processing. *Materials Today: Proceedings*, *62*, 191-197.

[84] Erfan, Y., & Kashani-Bozorg, S. F. (2011). Fabrication of mg/sic nanocomposite surface layer using friction stir processing technique. *International Journal of Nanoscience*, *10*(04n05), 1073-1076.

[85] Jabbari, A. H., Sedighi, M., Vallant, R., Huetter, A., & Sommitsch, C. (2015). Effect of pass number, rotational and traverse speed on particle distribution and microstructure of AZ31/SiC composite produced by friction stir processing. *Key Engineering Materials*, *651*, 765-770.

[86] Bagheri, B., Abdollahzadeh, A., Sharifi, F., & Abbasi, M. (2022). The role of vibration and pass number on microstructure and mechanical properties of AZ91/SiC composite layer during friction stir processing. Proceedings *of the Institution of Mechanical Engineers, Part C: Journal of Mechanical Engineering Science*, *236*(5), 2312-2326.

[87] Marode, R. V., Pedapati, S. R., Lemma, T. A., Loyte, A., Devarajan, Y., & Thandavamoorthy, R.

(2023). Influence of silicon carbide on microhardness and corrosion behavior of AZ91/SiC surface composites processed through friction stir processing: multi-response optimization using Taguchi-grey relational analysis. *Silicon*, *15*(16), 6921-6943.

[88] Abdollahzadeh, A., Bagheri, B., Abbasi, M., Sharifi, F., & Moghaddam, A. O. (2021). Mechanical, wear and corrosion behaviors of AZ91/SiC composite layer fabricated by friction stir vibration processing. *Surface Topography: Metrology and Properties*, *9*(3), 035038.

[89] Sagar, P. (2024). Synthesis and characterization of magnesium-titanium carbide nanocomposites via friction stir processing: An in-depth parameter investigation. *Proceedings of the Institution of Mechanical Engineers, Part C: Journal of Mechanical Engineering Science*, 09544062241234552..

[90] Vanam, J. P., Manjunadh, V., Kumar, A. S., Kumar, T. M., & Kishorebabu, N. (2023). Microstructure and mechanical properties of magnesium alloy reinforced with TiB2 and B4C processed through friction stir processing. *Materials Today: Proceedings*..

[91] Alam, N., Iqbal, M. M., Prakash, C., Singh, S., & Basak, A. (2020). Influence of the microstructural and mechanical properties of reinforced graphene in magnesium matrix fabricated by friction stir processing. In *Advances in Materials Science and Engineering: Select Proceedings of ICFMMP 2019* (pp. 235-247). Springer Singapore.

[92] Marode, R. V., Awang, M., Lemma, T. A., Pedapati, S. R., Hassan, A., Janga, V. S. R., ... & Devarajan, Y. (2024). Friction stir processing of AZ91 hybrid composites with exfoliated multi-layered graphene: A Taguchi-Grey relational analysis. *Journal of Alloys and Compounds*, *972*, 172703.